Preprint disclaimer

This manuscript is a non-peer reviewed preprint submitted to EarthArXiv (**https://eartharxiv.org**).

This version of the manuscript has been submitted for publication in Earth Science Reviews.

Please note that, although it may undergo peer review, it has not yet been formally accepted or published by the journal.

Future versions of this manuscript may differ slightly. If accepted, the final version will be available through the journal's website.

Please feel free to contact any of the authors; we welcome feedback and suggestions.

Document History

Version	Date	Action
1.0	[2025-07-16]	Submitted to EarthArXiv and Earth Science Reviews

Holocene relative sea-level changes from the Atlantic coast of South America

K. Rubio-Sandoval[1,2], T.A. Shaw[3], M. Vacchi[4], N.S., Khan[5], B.P. Horton[6], J.R. Angulo[7], M. Pappalardo[4], A.L. Ferreira-Júnior[8], S. Richiano[9], M.C. de Souza[7], P. C. Giannini[10], D.D. Ryan[4], E.J. Gowan[11,12], A. Rovere[1,13*]

1. MARUM - Center for Marine Environmental Sciences, University of Bremen, Bremen, Germany

2. Instituto de Geociencias, Universidad Nacional Autónoma de México, Querétaro, Mexico

3.Earth Observatory of Singapore, Nanyang Technological University, Singapore, Singapore

4. Department of Earth Sciences, University of Pisa, Italy

5. Department of Earth Sciences and Swire Institute of Marine Science, University of Hong Kong, Hong Kong, China

6. School of Energy and Enivronment, City University of Hong Kong, Hong Kong

7. Departamento de Geologia, Universidade Federal do Paraná, Paraná (UFPR), Brazil

8. Pós-graduação de Genética Evolutiva e Biologia Molecular, Universidade Federal de São Carlos (UFSCar), São Paulo, Brazil

9. Patagonian Institute of Geology and Paleontology, IPGP-CENPAT-CONICET, Argentina

10. Departamento de Geologia Ambiental e Aplicada, Instituto de Geociências, Universidade do São Paulo (USP), Brazil

11. Department of Earth and Environmental Sciences, Kumamoto University, Kumamoto, Japan

12. KIKAI institute for Coral Reef Sciences, Kikaijima, Japan

13. Department of Environmental Sciences, Informatics and Statistics, Ca' Foscari University of Venice, Venice, Italy

* Correspondence to: alessio.rovere@unive.it

Abstract

Holocene sea-level changes along the Atlantic coast of South America reflect a complex interplay between glacio-isostatic adjustment (GIA), regional tectonics, and local sedimentary processes. However, the uneven spatial and temporal resolution of existing sea-level data has hindered regional-scale assessments. Here, we compile and standardize 1108 relative sea-level (RSL) data points from Brazil, Uruguay, Argentina, and Chilean Tierra del Fuego, creating the first comprehensive Holocene RSL database for the southwestern Atlantic. The data reveal a widespread Mid-Holocene highstand between ~7000 and 4000 cal BP, with sea level rising 2 to 4 m above present, followed by a gradual fall to modern levels. This pattern is consistent with GIA model predictions across the region's >50° latitudinal span. Peak rates of RSL change occurred during the Early to Mid-Holocene transition, reaching up to 17.2 mm/yr in Tierra del Fuego and decreasing to 1.6 mm/yr near the Amazon delta. After ~5000 cal BP, RSL rates

decelerated, averaging –0.5 mm/yr into the Late Holocene. This standardized database fills a critical geographic gap and provides a robust framework for refining GIA models and understanding sea-level evolution since the Last Glacial Maximum in the Southern Hemisphere.

1. Introduction

The study of Holocene RSL changes is fundamental to understanding the behavior of sea level to ice melting,the subsequent isostatic response (e.g., Milne and Mitrovica, 2008; Björck et al., 2021), as well as other vertical land motions caused by factors such as tectonics or sediment compaction (e.g., Rabassa et al., 2000; Khan et al., 2015; Garrett et al., 2020). Most studies of Holocene RSL evolution trends are local in nature, as they report the age and elevation of sea level index points (SLIPs) at specific locations. However, there is a long-lasting effort in the sea-level community to standardize such data into sea-level databases with wider coverage (Tushingham and Peltier, 1992; Düsterhus et al., 2016; Khan et al., 2019; Rovere et al., 2023).

A renewed coordinated effort to build a global Holocene sea-level database was undertaken by the HOLSEA project (Khan et al., 2019), which promoted the use of rigorous standards for the reporting of sea-level data initiated in the late 80's and early 90's (van de Plassche, 1986; Pirazzoli, 1991; Shennan et al., 1993). The advantage of such standardization resides in the possibility to investigate spatial and temporal trends of RSL changes, enabling comparison with glacio isostatic adjustment models and, ultimately, to improve our knowledge on on the timing and modes of ice sheet melting since the last glacial maximum (LGM), in turn helping inform future sea-level rise scenarios (Horton et al., 2018). In the context of this new effort to standardize Holocene sea-level data globally, there is a notable spatial gap: the Atlantic coasts of South America, in the southwestern Atlantic.

The study of Holocene RSL changes in the southwestern Atlantic dates back to the 19th century. One of the earliest documented observations comes from Darwin (1851), who described above-present shoreline deposits along the Argentine coast. Shortly thereafter, in the Brazilian coastlines, Hartt (1870) identified sea urchin beds above the high tide level (HTL) in the area of Rio de Janeiro and interpreted them as indicators of higher sea levels. At the end of the 19th and beginning of the 20th centuries, John C. Branner drew initial paleo sea-level inferences for the Fernando de Noronha archipelago and the northeast Brazilian coast (Branner, 1889, 1890,1902, and 1904). Backeuser (1918) used rock-boring mollusks to estimate sea-level changes along the coastline between Rio de Janeiro and Santa Catarina.

However, it was not until the work of van Andel and Laborel (1964) that the earliest radiocarbon dates were published, enabling not only more reliable spatiotemporal paleo-sea-level reconstructions but also the quantification of the timing of sea-level changes allowing more reliable spatiotemporal paleo-sea-level reconstructions In the 1980s, Porter et al. (1984) quantified Holocene sea-level changes in Tierra del Fuego, Argentina, and Chile; and a decade later, the Holocene sea level variations in Uruguay began to be analyzed with the work of Bracco (1991) and Bracco and Ures (1998). Since then, sea level research in the southwestern Atlantic has evolved with several studies investigating more areas and progressively better

age control. More recent work investigated Holocene RSL variations due to GIA (e.g., Rostami et al., 2000; Milne et al., 2005).

Four seminal research papers summarizing Holocene RSL changes in the region present data with some degree of standardization and formed the starting point of our review. Angulo et al. (2006) compiled sea-level data along the Brazilian coastlines. They report and discuss the implications of more than 35 years of research by different groups and focus on sea-level variations in the mid to late Holocene. While highlighting discrepancies in the reported data, they describe a common trend of a mid-Holocene highstand with a subsequent fall to its present level. In Uruguay, Bracco et al. (2011) describe the origin and geomorphological history of the Castillos Lagoon deposits, whose elevations decrease from ~4 m to ~2 m above sea level (a.s.l.) from the mid to late Holocene. However, they also describe SLIPs at elevations lower than 1 m a.s.l. around 4500 years cal BP. Martínez and Rojas (2013) draw a sea-level curve based on data from beach ridge deposits, showing that the Uruguayan sea level was above the present level at approximately 6000 years cal BP and has been declining since then. Finally, Schellmann and Radtke (2010) present a wide review of SLIPs surveyed along the middle and south Patagonian Atlantic coast. According to the authors, beach ridges and valley-mouth terraces data show varying elevations throughout the Holocene. They estimate the Holocene sea-level transgression peaked at 6900 cal years BP, with RSL about 2-3 m a.s.l., and lasted until at least 6200 cal years BP, after which sea level declined to its present position. They also suggest that the mid and south Patagonian coast has likely been undergoing a slow glacio-isostatic uplift on the order of 0.3 - 0.4 mm/yr since mid-Holocene. Some of this uplift resulted from the deglaciation of the Patagonian ice sheet, which covered the Andes Mountains in Chile and Argentina. Though the volume of the Patagonian ice sheet was relatively small (< 1.5 m sea level equivalent at the LGM, Davies et al 2020; Gowan et al 2021b), it may impact the RSL history in southern South America (Björck et al., 2021).

Here, we expand upon the previous compilations of Milne et al. (2005) and Angulo et al. (2006) to make a new, standardized regional database of Holocene sea-level index points. Besides adding new datapoints that were not previously available, we standardized elevation measurement errors and indicative meanings and recalibrated radiocarbon ages following HOLSEA protocol, ensuring consistency and comparability with other datasets globally.

2. Regional setting

The sea-level database spans the southwestern Atlantic from the coasts of Brazil, Uruguay, Argentina, to the Chilean part of Tierra del Fuego (Figure 1A). The region of interest is located on the South America Plate and is, for the most part, a passive margin (see historical earthquakes location in Figure 1A). However, towards the northern part of Brazil (e.g., Pernambuco and Paraíba), several authors noted an increase in seismicity and highlighted the presence of faults offsetting Neogene deposits (Barreto et al., 2002; Bezerra and Vita-Finzi, 2000). In the far south, Tierra del Fuego is affected by the interaction between the Antarctic, Scotia, and South American plates (Isla and Angulo, 2016). Therefore, tectonics may play a role in the displacement of sea-level data in these two areas (Figure 1: regions 3 and 12). We divided our database into 12 regions (Figure 1A) based on data availability, geographic distribution and the increasing distance from the Antarctic ice sheet.

The area covered by the databas encompasses a variety of coastal environments along the southwestern Atlantic margin. These include estuaries, coastal lagoons, deltas, sandy beaches, and rocky shorelines, each with distinct sedimentary processes that influence the formation and preservation of sea-level indicators (Dominguez et al., 1990; Codignotto et al., 1992; Schellmann, 2002; Behling et al., 2004). In addition to this geomorphological variability, tidal regimes also differ across the region, along the Brazilian coast, tidal ranges span from microtidal conditions in the south to macrotidal in the northern regions, particularly in regions such as the Amazon River area (Melo et al., 2016). The Uruguayan coast is predominantly microtidal, with tidal amplitudes typically below 1 m (Martínez and Rojas, 2013). In contrast, much of the Argentine coast is mesotidal, with average tidal ranges around 1.7–2 m in open coast settings such as Mar del Plata (Santamaría-Aguilar et al., 2017).

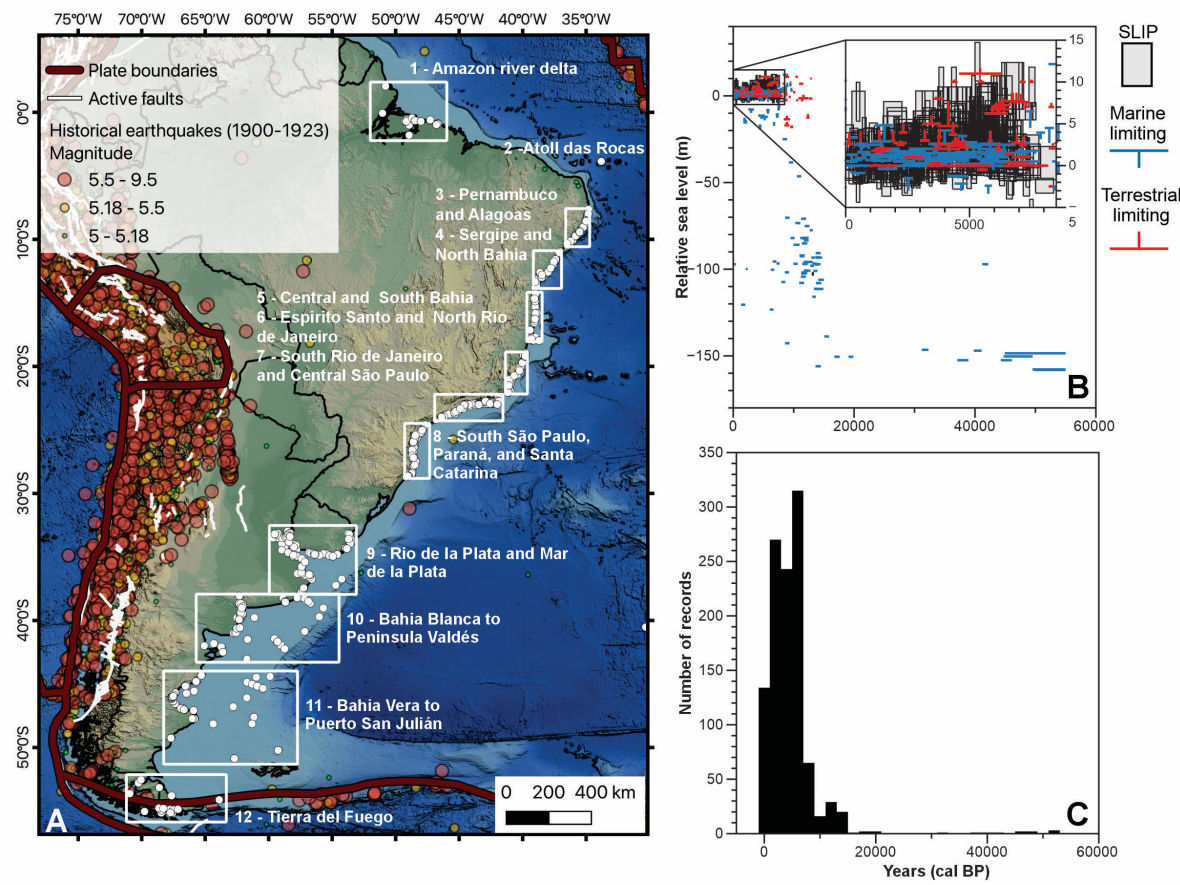

Figure 1. Spatio-temporal extent of the sea-level database. A) Regional subdivisions described in the text; white dots represent the location of SLIPs in each region. B) Age vs. RSL elevation plot for all the data points. C) Ages of the sea-level index points (SLIPs) included in the database. Credits: Base map from Ryan et al. (2009). Active faults from Styron (2019) and plate boundaries derived from Bird (2003), as modified by Hugo Ahlenius and Nordpil on GitHub (https://github.com/fraxen/tectonicplates). Historical earthquakes from US Geological Survey (2017).

3. Methods

The sea-level database was compiled following the standardized protocol developed by the HOLSEA project (Khan et al., 2019), following the approach described by van de Plassche (1986) and Shennan et al (2015). To be considered as valid SLIP, any geological, sedimentary, or biological facies must have four main attributes:

1. An accurate geographic location, and accurate elevation benchmarked to a tidal datum.
2. A well-constrained relationship between the indicator and paleo sea level.
3. The age of formation, traditionally obtained with radiometric dating techniques.

The main details on how the three points listed above were implemented in the database are detailed in the sections below.

3.1. Elevation of sea-level datapoints

In our database, we included the elevation of each SLIP and the defined vertical datum from the original works, wherever available. Overall, we identified the elevation and vertical datum combinations shown in Table 1. We account for potential sources of error in the measurement of a sample elevation following the criteria described in the database protocol by Hijma et al. (2015) (Table 2). If either the measurement method or vertical datum was not reported, we set the elevation error to 20% of the measured elevation, with a lower error limit of 0.2 m (for elevations between -1 m and +1 m) and an upper error limit of 2 m (for elevations higher than 10 m or deeper than -10 m). If neither the elevation measurement method nor the vertical datum was reported by the original publication, we set the elevation error to 40% of the measured elevation, with a lower error limit of 0.2 m (for elevations between -0.5 m and + 0.5 m) and an upper error limit of 2 m (for elevations higher than 5 m or deeper than -5 m).

Table 1. Combinations of elevation measurement methods and vertical datums reported in the database.

Elevation measurement method	Vertical datum	Number of occurrences
Not reported	Not reported	360
	Mean Sea Level / General definition	222
	Mean sea level from tidal data	51
	Nazaré Pier	4
	Vermetid biological datum	153
Total station or Auto/hand level	High Tide Level	82
	Mean Sea Level / General definition	6
Differential GPS	Local geoid	24
	Mean sea level from tidal data	17
	EGM 2008	7
	SAD-69	6
Handheld GPS	Mean Sea Level / General definition	8
Topographic map and digital elevation models	Mean Sea Level / General definition	7
Barometric altimeter	Local geoid	12
	Mean sea level from tidal data	8
	High Tide Level	3
	Not reported	3
	Mean Sea Level / General definition	2
Multibeam bathymetry data + core depth	Mean Sea Level / General definition	103
	Not reported	23
Dumpy level	Vermetid biological datum	7

Some studies, particularly those along the coasts of Patagonia, report elevations relative to the high tide level or "high tide mark". In these instances, the reported elevation was corrected to mean sea level by subtracting the difference between the local Mean Higher High Water (MHHW) and Mean Lower Low Water (MLLW) calculated using the IMCalc software (Lorscheid and Rovere, 2019).

Several studies along the Brazilian coasts report paleo sea level as the vertical distance between the modern and the fossil populations, bypassing the need to report sample elevation (e.g., Angulo et al., 2006; Toniolo et al., 2020). As elevation of a sample is a required field in the HOLSEA standardized format, we considered these reported values as sample elevations and assigned a 40% uncertainty, as no other information was available on either the originally adopted indicative range or the originally measured elevation. A note was inserted in the record for each of these SLIPs indicating the use of vertical distance in the original publication. A 40% uncertainty was also assigned for the Argentinian data reported by Codignotto et al. (1992), as little information on the elevation measurement is provided in the paper and previous studies.

Table 2. Sources of vertical uncertainties included in the database. Each vertical uncertainty was applied as appropriate to different samples. SLIP: Sea-Level Index Point; RTK GPS: Real-Time Kinematic Global Positioning System; DEM: Digital Elevation Models. * Specifications.

Core samples or sections	
Source of uncertainty	**Description**
Sample thickness uncertainty	Half of the sample thickness
Sampling uncertainty	Depth range of the dated sample
	± 0.01 m if not specified
Core shortening/ stretching uncertainty	± 0.15 m for rotatory/vibracoring
	± 0.05 m for hand coring
	± 0.05 m for hand coring
	± 0.01 m for Russian sampler
	Assigned largest uncertainty (± 0.15 m) if type of corer was unclear
Non-vertical drilling uncertainty	2% (e.g., 0.02 m/m depth)
Outcrops or other type of paleo-sea level indicators	
Tidal uncertainty	Half of the tidal range
	Applies only to samples collected offshore with reference to the water's surface*
Water depth uncertainty	Uncertainty associated with the measurements of water depth, as reported
	± 0.05 m if not specified
Levelling uncertainty	± 0.01 m for high-precision levelling equipment (e.g., total station, dumpy level)
	± 0.03 m if levelling method is unknown, but the authors mentioned elevations measured/surveyed
	± 20% or 40% of reported elevations if further uncertainties regarding the SLIP levelling
GPS or RTK uncertainty	Uncertainty associated with RTK GPS measurements, as reported
	± 0.1 m if not specified
Benchmark uncertainty	± 0.1 m for reliable and stable benchmarks
	± Precision of benchmarks if further uncertainties
	Does not apply to samples that were not levelled to a benchmark*
Vegetation zone uncertainty	± 20% of the reported elevation range of vegetation
	Applies only to samples whose elevations were estimated from vegetation zones*
Map uncertainty	± 0,50 m for high-precision levelling (additional elevation methods are included)
	± 1 m if only a topographic map were used to determine sample elevation
DEM uncertainty	± 0,50 m (as recommended by Hijma et al., 2015 for areas with significant relief)

3.2. Indicative meaning of sea-level indicators

The relationship between a sea-level indicator and the past sea level is known as the indicative meaning, comprising the Indicative Range (IR), and the Reference Water Level (RWL). The IR represents the vertical elevation range occupied by a sea-level indicator relative to contemporary tidal datums. The RWL is the midpoint of the IR.

The database includes several indicators defining the discrete position of past RSL (Figure 2, 3, and Table 3 for details). The database also includes limiting data points, which provide an upper (terrestrial limiting) or lower (marine limiting) bound against the past RSL position (Shennan et al., 2015; Khan et al., 2019). In our work, we have reviewed in detail all published RSL evidence and allocated each SLIP with an indicative meaning. If the information provided in the original literature was insufficient to quantify the indicative meaning through direct comparison with a modern analog, we calculated it using the IMCalc software (Lorscheid and Rovere, 2019). For beach ridges in Argentina and Uruguay, created by wave runup processes (Rovere et al., 2025), we calculate the indicative meaning using modern wave data and a set of wave runup models to estimate their lower (ordinary berm) and upper limits (higher storm berm). Through this process, we calculated the 2% exceedance wave runup level using the different models implemented into the py-wave-runup tool coded by Leaman et al. (2020) following the methodology employed in Rubio-Sandoval et al. (2024).

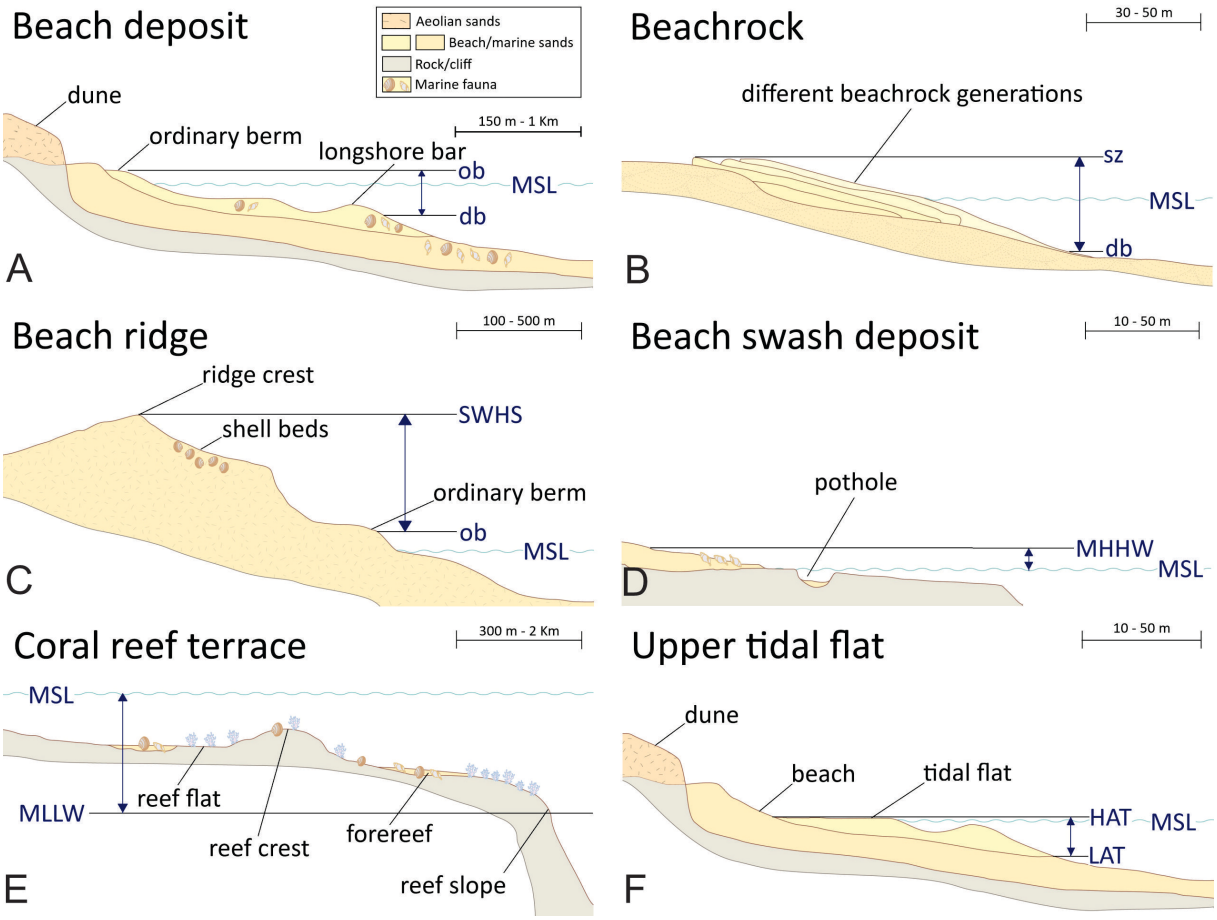

Figure 2. Schematic illustration of the paleo-sea level indicators with their upper and lower limits of the Indicative Range shown by the black lines and blue arrows (see Table 1 for more details and definitions). A) to F) schemes of paleo-sea level indicators. db: breaking depth; ob: ordinary berm; sz surf zone; MSL: mean sea level; SWHS: storm wave swash height; MHHW: mean higher high water; MLLW: mean lower low water; HAT: highest astronomical tide; LAT: lowest astronomical tide.

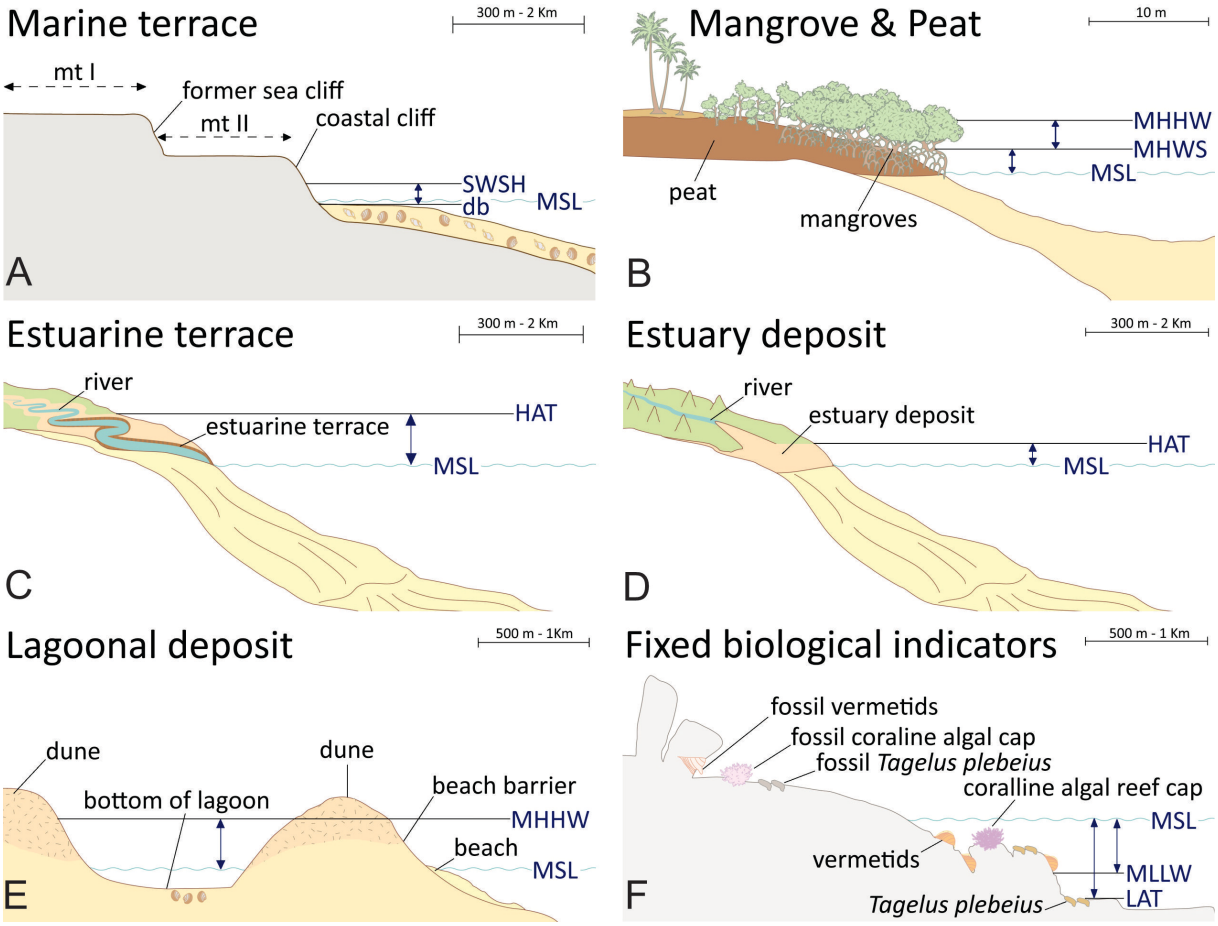

Figure 3. Schematic illustration of the paleo-sea level indicators with their upper and lower limits of the Indicative Range shown by the black lines and blue arrows (see Table 1 for more details and definitions). A) to F) schemes of paleo-sea level indicators. mtI: marine terrace I; mtII marne terrace II; db: breaking depth; ob: ordinary berm; sz surf zone; MSL: mean sea level; SWHS: storm wave swash height; MHHW: mean higher high water; MHWS: mean high water springs; MLLW: mean lower low water; HAT: highest astronomical tide; LAT: lowest astronomical tide.

The models used to calculate the indicative meaning of beach ridges require as input the beach slope, significant wave height, and period. We determined the beach slope at four areas where beach ridges were reported in literature (i.e. Río de la Plata delta, Bahia Blanca to Peninsula Valdés, Bahia Vera to Puerto San Julián, and Tierra del Fuego) using the CoastSat.Slope toolbox (Vos et al., 2019, 2020). This toolbox analyzed Landsat and Sentinel satellite data between 2000 and 2023, alongside tides extracted from the FES2014 global tidal model (Lyard et al., 2021; Carrere et al., 2016). To calculate wave height and period we used the RADWave tool (Smith et al., 2020), which allows the querying of satellite altimetry data. We extracted a time series of wave data between 66°W to 70°W and 38°S to 52°S, in a period included between Jan 1st, 2000, and Jan 1st, 2023. For the same time frame, we queried the FES2014 model and extracted water levels at a 15-minute interval. By coupling tidal and wave data via their UTC timestamps, we gathered a database with 231462 wave conditions. We selected a beach slope sampled from a normal distribution created with the mean and standard deviation of the beach slope for each condition. We used the "ensemble" function of py-wave-runup to run for each wave height and period eight different runup models (Supplementary Figure 1). We added (or subtracted) the corresponding water level at each calculated runup.

Table 3. Types of paleo-sea level indicators in the database, including their indicative range and number of occurrences. MLLW=Mean Lower Low Water; MHHW=Mean Higher High Water; MSL=Mean Sea Level; LAT=Lowest Astronomical Tide; HAT=highest astronomical tide; MHWS=Mean High Water Springs; GWL=Groundwater Level. * Denotes indicative ranges provided by the revised publications.

Primary indicator type	Secondary indicator type	Indicative range	Number of data points
Beach deposit	Beach deposit or beachrock	Breaking depth to ordinary berm	68
		MLLW-MHHW*	1
	Beach ridge	Back calculated from values reported by the original authors*	51
		Ordinary berm to storm wave swash height	287
	Beach swash deposit	MHHW-MSL	1
Fixed biological indicators	Coral reef terrace or Coralline algal reef cap	MSL - MLLW	17
	Tagelus plebeius	LAT to MSL	2
	Vermetids	MLLW to MSL	177
Marine terrace	Marine terrace	Breaking depth to storm wave swash height	33
Sedimentary	Basal peat (non-mangrove)	MHHW to MSL	2
	Estuarine terrace (preserved tidal flat surface)	MSL to HAT	28
	Estuary deposit	HAT to MSL	2
	Lagoonal deposit	MHHW to MSL	2
	Mangrove	Measured on modern analog*	5
		MSL to MHWS	19
	Upper Tidal Flat	LAT to HAT	4
The data point is a marine or terrestrial limiting indicator		N/A	409

3.3. Radiometric ages

In our database, the ages of all sea level indicators were determined using radiocarbon dating (^{14}C). As the production of atmospheric radiocarbon has varied through geological time, we recalibrated all radiocarbon ages reported in the literature into sidereal years with a 2σ range. Age calibrations were done using CALIB software (version 8.2). We use the Marine20 curve to calibrate marine and estuarine samples, and the SHcal20 curve for terrestrial samples (Stuiver and Polach, 1977; Heaton et al., 2020; Reimer et al., 2020, Hogg et al., 2020). Marine reservoir corrections have been applied according to the closest available data for each study area (Macario et al., 2023). When a study site was in an area with unknown Delta-R values, we used the Marine Reservoir Correction Database (Reimer and Reimer, 2001). Following the analysis by Hu (2010) of ^{14}C ages from bulk peat samples, a ±100 ^{14}C yr error was applied to account for sample contamination (Törnqvist et al., 2015). Codignotto et al. (1992), Björck et al. (2021), and Fasano et al. (1983) reported calibrated ages; therefore, we did not re-calibrate them.

All SLIPs in our database are presented as calibrated years before present (yr BP), where year 0 is AD 1950 (Stuiver and Polach, 1977). A concern with old radiocarbon ages is the correction for isotopic fractionation (Törnqvist et al., 2015). This correction became a standard procedure

at most laboratories by the late 1970s (Stuiver and Polach, 1977), but some laboratories have only applied this correction since the mid-1980s (Hijma et al., 2015). When needed, we reported the values described by the authors or the marine carbonate standard ± 3 ‰ (Törnqvist et al., 2015). Further details and choices made while compiling the radiocarbon ages (e.g., lab code or whether a $\delta^{13}C$ fractionation correction was added) are available in the database (see supplementary file).

3.4 Data rejection criteria

Data points were rejected when there was insufficient information within the original sources, such as the elevation of a sample. For example, when the depth of a sample within the core was reported but not the core top elevation, we had to reject the data point. Marine samples with ^{14}C age adjusted for Delta R < 603 were rejected because they were not valid for the calibration curve (Stuiver and Polach, 1977). Another reason for rejection, only if strictly necessary, was if a SLIP was at odds regarding the RSL estimate with coeval data points in the same region. However, rejected data points and associated radiocarbon ages were not eliminated from the database and are available for future reassessment in case further information arises. We remark that assigning high uncertainties and rejection of a data point does not reflect the quality of the published papers where the data points are reported. The uncertainty assigned and the rejection of a data point were exclusively designed to discern the suitability of each record to be used as a standardized SLIP or limiting point.

3.5. Statistical model of Holocene RSL and Glacial isostatic adjustment

To quantify sea-level for each region identified within the database (see sections 4.1 and 4.2 for details), we applied the Spatio-Temporal Empirical Hierarchical Model (STEHM) by Ashe et al. (2019) to the SLIPs data.

To analyze the RSL trends in the database in comparison with predicted RSL histories, we use GIA model sea level predictions forced by different ice models. We use the SELEN code to calculate RSL (Spada and Stocchi, 2007; de Boer et al., 2014, 2017). SELEN assumes the Earth's rheology is spherically symmetric with an elastic lithosphere and a Maxwell viscoelastic mantle and calculates sea level using a constant time step. This version of SELEN also considers migrating shorelines and Earth's rotational effects. In this study, we compute the sea level at 500-year time steps.

The first ice model we employ in our comparison is ICE-6G_C (VM5a) (hereafter referred to as ICE6G) (Argus et al., 2014; Peltier et al., 2015). The version of the model we use includes a global ice sheet history spanning the past 122000 years. The time step for this model is not constant and is larger than 500 years prior to 21000 years cal BP, so we linearly interpolate the ice sheet thickness between the time steps. The ice volume of the ICE6G model was tuned to a paleo sea level record from Barbados and refined to fit present-day vertical land motion in areas covered by Late Pleistocene ice sheets. The VM5a Earth model that was used in conjunction with ICE6G has a 60 km thick lithosphere, a 40 km thick layer below the lithosphere with a viscosity of 1×10^{22} Pa s, a 5×10^{20} Pa s upper mantle, a 1.6×10^{21} Pa s lower mantle between 660 and 1160 km depth, and the rest of the lower mantle with a viscosity of 3.2×10^{21} Pa s. Peltier et al. (2015) used the Holocene sea-level indicators from southeastern South America, as compiled in Rostami et al. (2000), to evaluate the ICE6G model. They

attributed the Holocene highstand position to rotational effects. By including rotational effects, the calculated sea level from ICE6G was better able to match the highstand in many locations along the eastern South American coast. The Patagonian Ice Sheet in ICE6G has a sea level equivalent ice volume of 0.9 m at the LGM, which decreases to its present-day value at 15,500 years cal BP.

The second ice model we employ is the PaleoMIST 1.0 reconstruction (Gowan et al., 2021b). This model was designed as a preliminary ice sheet and topography reconstruction for the past 80000 years, at 2500-year time steps. The Earth model used with PaleoMIST has a 120 km thick lithosphere, 4×10^{20} Pa s upper mantle, and 4×10^{22} Pa s lower mantle. The ice thickness has been linearly interpolated to 500-year time steps for the calculations in this study. The model was tuned with sea level observations from the Laurentide and Eurasian ice sheets, and was not rigorously evaluated against far-field sea level records such as those in eastern South America. Some initial calculations for southeastern South America presented by Gowan et al. (2021a) demonstrated that the sea level highstand may not have happened simultaneously along the coast. Subsequent analysis of PaleoMIST 1.0 demonstrated that the ice volume during the Mid to Late Holocene is too great to account for far-field sea level observations (Gowan, 2023). Almost all of this excess ice volume is located in Antarctica, so in this paper, we have modified PaleoMIST 1.0 to use the present-day Antarctica ice sheet configuration from 5000 years BP to mitigate this issue. The Patagonian Ice Sheet in PaleoMIST has a sea level equivalent ice volume of 0.8 m at the LGM, which decreases to present-day values at 12,500 years cal BP.

4. Results

The spatial extent covered by the database spans between 0° and 60° latitude South and between 40° and 70° longitude West (Figure 1). We reviewed data from 132 studies published between 1964 and 2023 to gather 1108 valid data points (701 SLIPs, 100 terrestrial and 307 marine limiting points); each associated with a temporal and vertical uncertainty. We rejected 291 data points because the necessary information required by the standard sea-level database protocols was not achieved. The database spans the last 12000 years cal BP, with nearly 80% of the data younger than 10000 years cal BP (Figure 1C). Most radiocarbon age errors are lower than 500 years, and RSL elevation uncertainties (including elevation error and indicative meaning uncertainty) are between 0.5 m and 2 m.

4.1. Brazil

4.1.1. Region 1: Amazon River delta

The region encompassing the Amazon River delta area is in northern Brazil, between Amapá and Pará states (Figure 4A). Within this region, we reviewed 27 SLIPs and 15 limiting data. The main SLIPs are from mangroves (Cohen et al., 2005; Behling et al., 2001), estuarine deposits (Behling et al., 2004; Cohen et al., 2012), upper tidal flats (Cohen et al., 2012; Guimarães et al., 2012), and basal peat (non-mangrove) (Ribeiro et al., 2023).

The record in the Amazon River delta dates back to the Early Holocene, with some terrestrial limiting data placing RSL below 0 m (Figure 4B). The oldest SLIP in this region places RSL at -6 ± 1.9 m at ~7500 years cal BP (ID: 748). Younger SLIPs indicate RSL rose to a peak at 1.6 ± 1.4

m at ~5000 years cal BP, followed by an oscillation between -0.6 ± 1.2 m b.s.l. (3900 years cal BP) and 0.7 ± 1.1 m a.s.l (400 years cal BP) (Figure 4B). One SLIP (ID: 734) documents a high RSL value of ca. 2.9 ± 1.4 m a.s.l. at ~600 years cal BP.

The STEHM shows an increase in the RSL during the Mid-Holocene (from ~8000 to ~5000 years cal BP) at an average rate of 1.6 mm/yr. After 5000 cal BP, the rate of RSL change slowly decayed through the Late Holocene at a mean rate of -0.5 mm/yr (Figure 4B, D). The GIA prediction from the ICE6G model fits the data, while PaleoMIST model seems to underestimate RSL at the beginning of the Mid-Holocene (Figure 4B).

4.1.2. Region 2: Atol das Rocas

The Atol das Rocas is an atoll island located 250 km offshore the northeastern Brazilian coast. In this region we reviewed 25 SLIPs and 6 limiting data (Figure 4C). The predominant paleo-sea level indicators are coral reef terraces (Gherardi and Bosence, 2005), beach deposits, and one lagoonal deposit (Angulo et al., 2022a; Kikuchi and Leao, 1997).

In Atol das Rocas there is an absence of Early Holocene data. From 3000 years cal BP to the present, SLIPs are scattered but indicate that the local sea level in this region was above present level, on average, +1.6 m (Figure 4C).

The STEHM model shows a gradual decrease in relative sea level over the last 3000 years, with an average rate of about –0.5 mm/yr, a slight rise around 150 cal BP indicates a temporary change in sea-level trends (Figure 4C, E). GIA model predictions show that the sea level in this region was already close to its modern position around 5000 years cal BP, and GIA predictions are significantly lower than the observed RSL in the region, however remaining within the error bars of the SLIPs and the STEHM (Figure 4C).

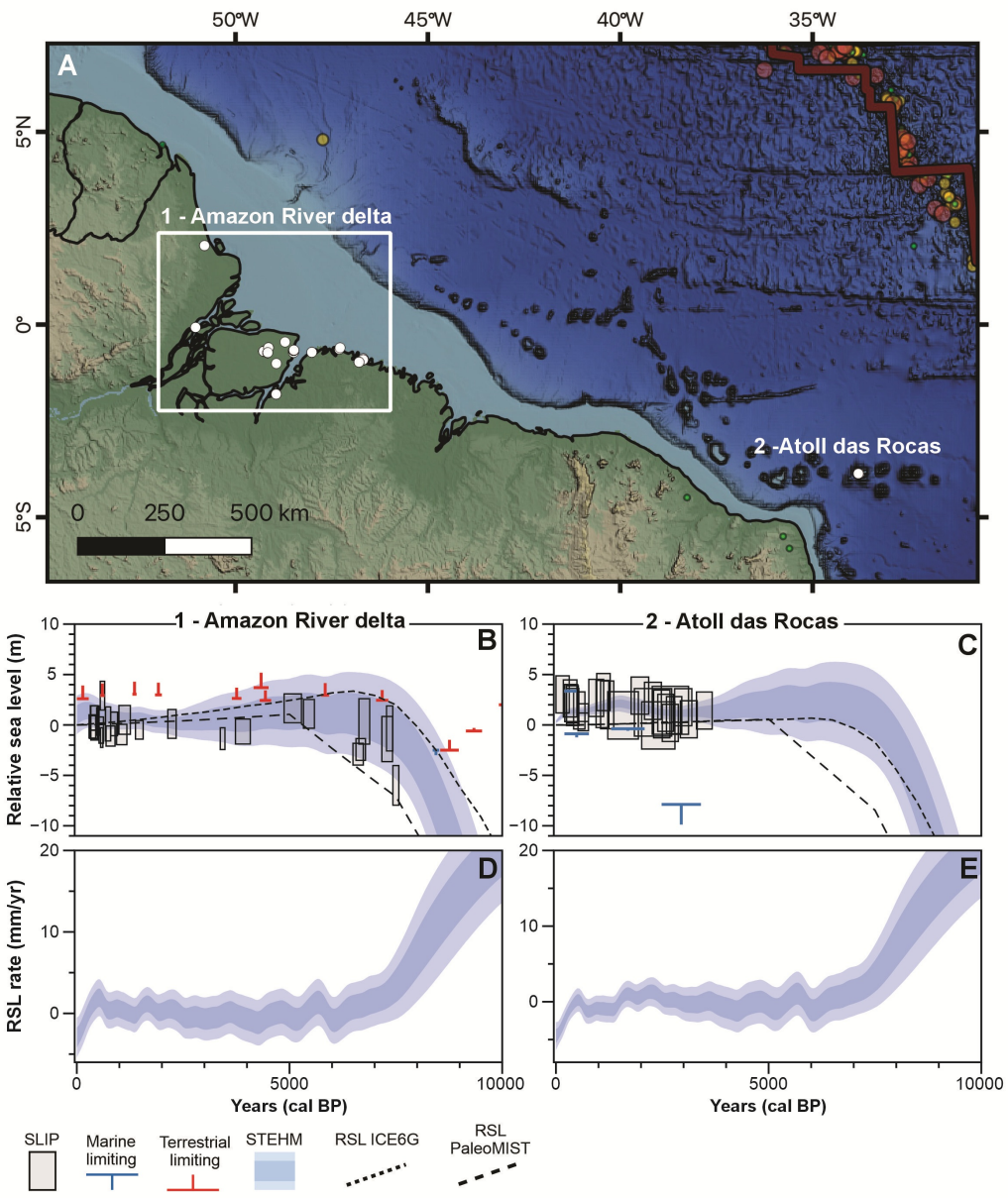

Figure 4. Map (A) and RSL reconstructions (B-E) and rates from regions 1 and 2 using the spatio-temporal model. For all plots, the model mean and 2σ uncertainty are represented by a solid line and shaded envelopes, respectively. SLIPs (grey boxes) are plotted as calibrated age against RSL to the present. Limiting points are plotted as an "inverted-T" red symbol for terrestrial or an "T" blue symbol for marine. The dimensions of boxes and symbols for each point are based on elevation and age (2σ) errors. SLIP: sea-level index point; STEHM: spatio-temporal empirical hierarchical model; ICE6G (short, dashed line) and PaleoMIST (large, dashed line) represent the GIA models. Credits for the base map in A) are the same as Figure 1A.

4.1.3. Region 3: Pernambuco and Alagoas

In this region, we reviewed 31 SLIPs, and 33 limiting data (Figure 5B). Vermetid rims are the dominant paleo-sea level indicators (Martin et al., 1996; Dominguez et al., 1990; Angulo et al., 2006), although beach deposits (Dominguez et al., 1990), two data points from mangroves (Barbosa et al., 1986), and one from a coralline algal reef cap (Delibrias and Laborel, 1971; Laborel, 1969) were also described.

The records in Pernambuco and Alagoas date back to the Mid-Holocene. The oldest SLIP (ID: 143) places RSL at 0.3 ± 1.9 m a.s.l. at ~7800 years cal BP. Younger SLIPs indicate RSL rose to

ca. 5 m ± 1.8 m at 3800 years cal BP and has oscillated since, between -0.4 ± 0.4 m b.s.l. (3200 years cal BP) and 2.3 ± 0.8 m a.s.l (200 years cal BP) (Figure 5B).

According to the STEHM, after the Mid-Holocene RSL highstand (around 6000 years cal BP), RSL falls to its present position at a mean rate of -0.5 mm/yr (Figure 5B, E). The GIA prediction from the model ICE6G fits the data, while PaleoMIST seems to underestimate the RSL at the beginning of the Mid-Holocene (Figure 5B).

4.1.4. Region 4: Sergipe and North Bahia

In the Sergipe and North Bahia region, we reviewed 35 SLIPs, and 16 limiting data (Figure 5C). In this region, there are three types of paleo-sea level indicators: vermetid rims (Bittencourt et al., 1978; Martin et al., 1979,1980; Delibrias and Laborel, 1971; Angulo et al., 2006), beach deposits (Bittencourt et al., 1978; Martin et al., 1979/1980), and mangroves (Martin et al., 1979/1980; Martin et al., 1982).

The records in Seguipe and North Bahia date back to the early Holocene. The oldest SLIP (ID: 152) places the RSL at −2.4 ± 0.8 m b.s.l. at 8000 years cal BP (Figure 5C). From there, the RSL increases to ~1.7 ± 1.9 m a.s.l. ca. 5700 years cal BP. One data point (ID: 211) stands out, recording the highest RSL value of 5 ± 1.9 m a.s.l. at ~5400 cal years BP. However, this unusually high value appears inconsistent with the general trend and should be carefully re-evaluated to confirm its reliability. Younger SLIPs in this region plot RSL between ~3 to ~2 m a.s.l. between 4000 to 2000 years cal BP, after which it falls close to its modern position (Figure 5C).

According to the STEHM RSL rose between ~6000 and ~4300 cal years BP, with rates of change gradually decreasing from about 6.7 mm/yr to -0.4 mm/yr, reflecting a slowdown in the rise during this period. During the Late Holocene, RSL showed a general trend toward stabilization with minor fluctuations and lower rates of change close to 0 mm/yr (Figure 5C, F). The GIA prediction from the model ICE6G fits the data, while PaleoMIST seems to underestimate the RSL at the beginning of the Mid-Holocene (Figure 5C).

4.1.5. Region 5: Central and South Bahia

In the region encompassing Bahia state's central and southern sectors, we reviewed 37 SLIPs and 20 limiting data (Figure 5D). The sea-level indicators identified in this region consist of beach deposits (Angulo et al., 2022b), vermetid rims (Bittencourt et al., 1978; Martin et al., 1979/1980; Martin et al., 1996; Angulo et al., 2006; 2022b), and mangroves (Fontes et al., 2017; Cohen et al., 2020).

The record of this region dates to the Mid-Holocene. RSL changes in this region show slight oscillations over time, with values ranging from 4 m a.s.l. to -0.9 m b.s.l. Two data points (IDs: 249; 1214) show the highest RSL values (4.3 ± 1.6 m a.s.l. and 4.5 ± 1. 7 m a.s.l, respectively) at around 5000 years cal BP (Figure 5D).

The STEHM shows a rising sea level between 8000 to ~4000 years cal BP with a mean rate of change of 1.8 mm/yr. From the Late Holocene onward, sea level gradually fell at rates around –0.5 to –1 mm/yr, marking a slow regression (Figure 5D, G). The GIA model predictions of

ICE6G show a good agreement with the RSL history reconstructed by the STEHM, while PaleoMIST underestimates the trend at the beginning of the Mid-Holocene (Figure 5D).

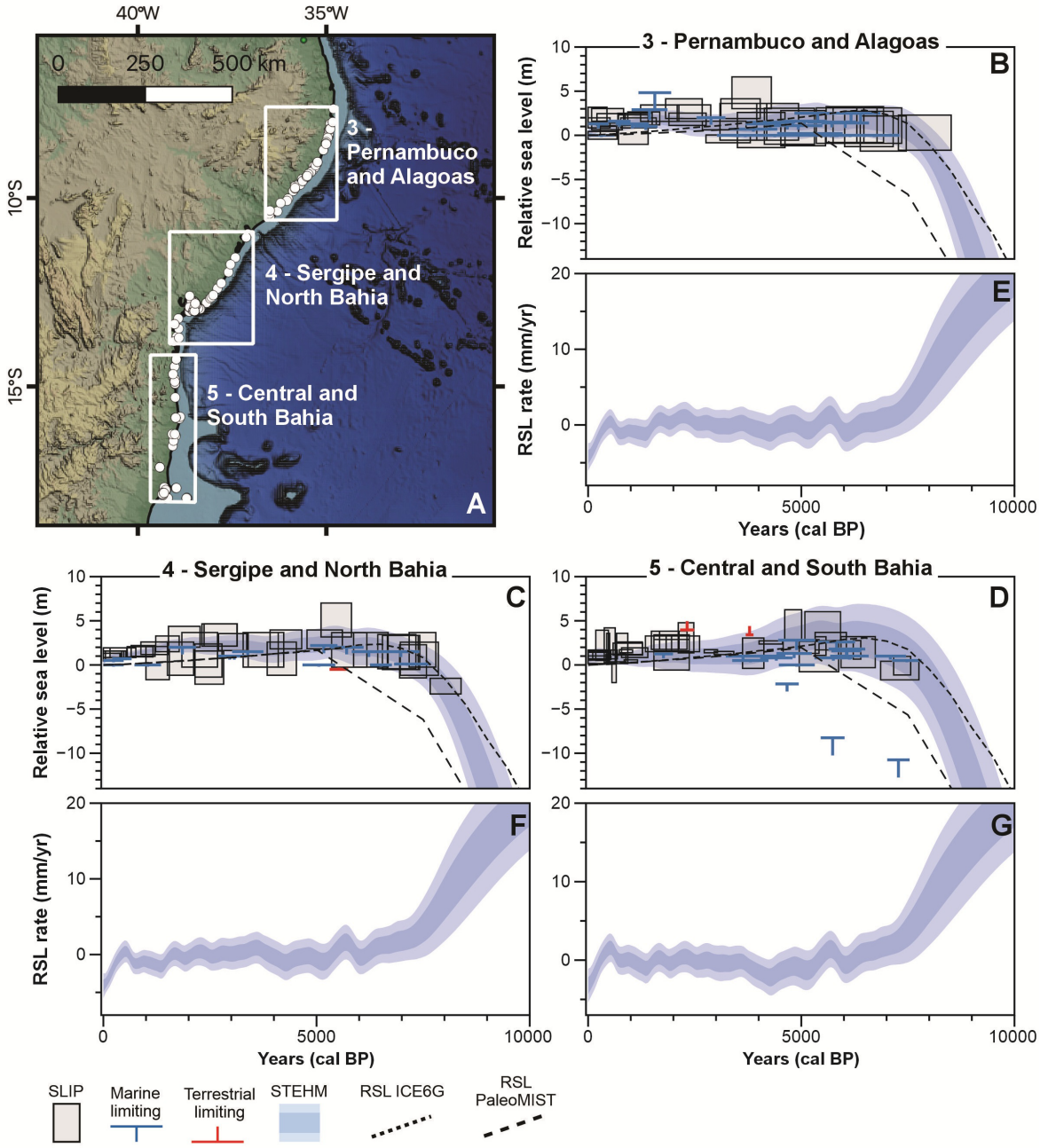

Figure 5. Map (A) and RSL reconstructions (B-G) and rates from regions 3, 4, and 5 using the spatio-temporal model. For all plots, the model mean and 2σ uncertainty are represented by a solid line and shaded envelopes, respectively. Index points (grey boxes) are plotted as calibrated age against changes in sea level relative to the present. Limiting points are plotted as an "inverted-T" red symbol for terrestrial or an "T" blue symbol for marine. The dimensions of boxes and symbols for each point are based on elevation and age (2σ) errors. SLIP: sea-level index point; STEHM: spatio-temporal empirical hierarchical model; ICE6G (short, dashed line) and PaleoMIST (large, dashed line) represent the GIA models. Credits for the base map in A) are the same as Figure 1A.

4.1.6. Region 6: Espírito Santo and North Rio de Janeiro

Twelve SLIPs and 48 limiting data were reviewed in this region (Figure 6B). Therefore, RSL history of this region is based primarily on limiting data (Delibrias and Laborel, 1971; Martin

and Suguio, 1989; Martin et al., 1996; Martin et al., 1997). The few SLIPs identified include vermetid rims (Martin and Suguio, 1989; Martin et al., 1996; Angulo et al., 2006, 2016), and one associated with a beach deposit (Martin et al., 1996; Martin et al., 1997).

The record of this region dates back to the Mid-Holocene. The marine limiting data suggest that RSL was already above present ca 7000 years cal BP. The oldest SLIP (ID: 347) places the sea level at 1.7 ± 0.6 m a.s.l. at ~6000 years cal BP. Sea level reached a peak of 3.6 ± 1.3 m asl around 5000 years cal BP. RSL oscillated around 3 m until 3000 years cal BP after which it began a falling trend to the present (Figure 6B).

The STEHM shows a rising sea level between ~8000 and ~5000 cal yr BP. During this period, the rate of RSL change reaches a maximum, with an average value of approximately 1.7 mm/yr. After this rise, the RSL falls at a mean rate of -0.3 mm/yr, into the Late Holocene (Figure 6B, E). ICE6G GIA predictions fit the data, while PaleoMIST predictions are lower until ca. 5000 years cal BP (Figure 6E).

4.1.7. Region 7: South Rio de Janeiro and Central São Paulo

In this region, we reviewed 62 SLIPs and 47 limiting data (Figure 6C). Despite the large number of SLIPs, only two types of indicators were described in this region: vermetid rims (Delibrias and Laborel, 1971; Martin and Suguio, 1978; Suguio and Martin, 1978; Flexor and Martin, 1979; Martin et al., 1979; Martin et al., 1979/1980; Suguio et al., 1980; Martin et al., 1996; Angulo et al., 2006; Castro et al., 2014; Angulo et al., 2016; Baptista de Jesus et al., 2017; Castro et al., 2021), and beach deposits (Martin et al., 1979; Martin and Suguio, 1989; Angulo et al., 2006; Castro et al., 2014; Angulo et al., 2016; Castro et al., 2021).

The record in this region mainly corresponds to the Mid-Holocene. There are only two marine limiting data from the early Holocene, which indicate a sea level of ca. -15 m b.s.l. (Figure 6C). The mid-Holocene data suggest that from ~7000 to 5000 years cal BP, sea level was close to the present mean sea level, averaging ~1.1 m a.s.l. Just one SLIP (ID: 464) shows a higher RSL value (2.3 ± 1.5 m a.s.l.) ca. 5800 years cal BP. This regional record shows Mid-Holocene sea level peaked ca. 4900 years cal BP at 3.8 ± 1.4 m a.s.l. Still, one SLIP (ID: 463) indicates a higher RSL (4.7 ± 2.2 m a.s.l.) at 3300 years cal BP. After this time, RSL falls gradually towards its modern position (Figure 6C).

The STEHM shows a rapid sea level rise between 8000 and 6000 years cal BP, with rates peaking around 7.2 mm/yr, followed by a gradual deceleration in sea level rise from 6000 to 4000 years cal BP (mean value of -0.7 mm/yr). During the Late Holocene, RSL stabilizes near present-day levels, with rates fluctuating around zero (Figure 6C, F). ICE6G GIA predictions fit the data, while PaleoMIST predictions are lower at the beginning of the Mid-Holocene (Figure 6C).

4.1.8. Region 8: South São Paulo, Paraná, and Santa Catarina

In South São Paulo, Paraná, and Santa Catarina states, we reviewed 61 SLIPs and 32 limiting points (Figure 6D). All the reported paleo-sea level indicators in this region are vermetid rims (Angulo, 1989;1992; Angulo et al., 1999; Souza et al., 2001; Angulo et al., 2002; Toniolo et al., 2020; Angulo et al., 2022c).

The record in South São Paulo, Paraná, and Santa Catarina date back to the Mid-Holocene. The oldest SLIP (ID: 544) places the sea level at 2.3 ± 0.8 m a.s l. at 5600 years cal BP. The highest sea level value is observed around 5000 years cal BP at ca. 3.8 ± 1. 4 m a.s.l. Since then, the RSL gradually falls towards the present, ranging from ~3.3 ± 1.0 m a.s.l. to ~0.4 ± 0.3 m a.s.l. (Figure 6D).

The STEHM shows a rapid RSL rise culminating in a highstand around 6000 years cal BP, with rates reaching up to ~5 mm/yr. Following this highstand, the RSL progressively falls during the Late Holocene, with rates gradually decreasing from ~1 mm/yr to near 0 by 2000 years cal BP (Figure 6D, G). The GIA model predictions of ICE6G fit the data; PaleoMIST predictions are lower than the RSL trend described by the STEHM during the beginning of the Mid-Holocene (Figure 6D).

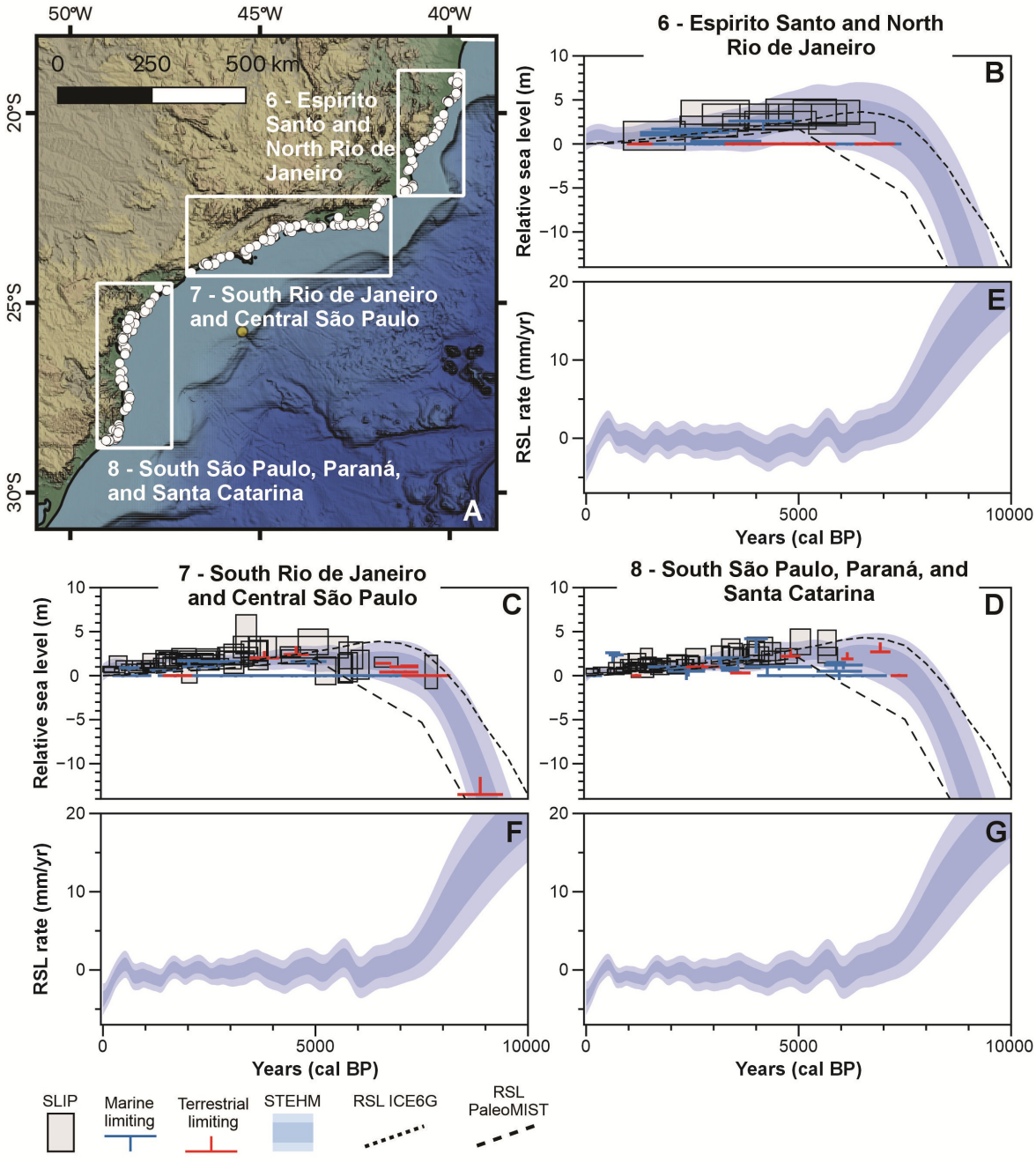

Figure 6. Map (A) and RSL reconstructions (B-G) and rates from regions 6, 7, and 8 using the spatio-temporal model. For all plots, the model mean and 2σ uncertainty are represented by a solid line and shaded envelopes, respectively. Index points (grey boxes) are plotted as calibrated age against changes in sea level relative to the present. Limiting points are plotted as an "inverted-T" red symbol for terrestrial or an "T" blue symbol for marine. The dimensions of boxes and symbols for each point are based on elevation and age (2σ) errors. SLIP: sea-level index point; STEHM: spatio-temporal empirical hierarchical model; ICE6G (short, dashed line) and PaleoMIST (large, dashed line) represent the GIA models. Credits for the base map in A) are the same as Figure 1A.

4.2. Uruguay – Argentina

4.2.1. Region 9: Río de la Plata delta

In this region, we reviewed 169 SLIPs and 28 limiting data (Figure 7B). The main paleo-sea level indicators described in the region were beach ridges (Cortelezzi, 1977; Albero and Angiolini, 1983; Guida and González, 1984; Codignotto et al., 1992; Cortelezzi et al., 1992; Aguirre, 1993; Colado et al., 1995; Cavallotto, 1995; Cavallotto, 2002; Bracco and Ures, 1998; Bracco, 2000; Bracco et al., 2011; Martínez and Rojas, 2013; Prieto et al., 2017; Cavallotto et al., 2004; Cavallotto et al., 2005; Martínez et al., 2006) and estuary deposits (Albero and Angiolini, 1983; Fasano et al., 1983; González and Ravizza, 1987; Figini, 1992; Martínez et al., 2006; Amato and Busso, 2009; Prieto et al., 2017; Fucks and De Francesco, 2003). One upper tidal flat deposit, one beach swash deposit (Bracco and Ures, 1998; Prieto et al., 2017), and two biological indicators (deposits containing remnants of the mollusk *Tagelus plebeius*) were also described (Bracco et al., 2011).

The record in Rio de la Plata delta mainly corresponds to the Mid-Holocene; only one terrestrial limiting data suggests that RSL was -18 m b.s.l. during the Early Holocene (Supplementary Figure 2). The oldest SLIP (ID: 296) places the sea level around 3.1 ± 0.6 m a.s.l. at 6800 years cal BP. Two SLIPs (IDs: 47; 269) show the highest RSL value ~4.7 m a.s.l. at 5300 years cal BP and 4900 years cal BP, respectively. Since then, the data shows an almost continuous RSL fall (Figure 7B).

The STEHM, the RSL reached its highstand around 7000 cal years BP, followed by a progressive fall with rates decreasing from about 3.7 mm/yr to near 0. During the Late Holocene, the RSL continued to decline, but at much slower and more variable rates, fluctuating between approximately +1 mm/yr and -3 mm/yr (Figure 7B, D). Both GIA models fit the data from 8000 cal BP to the present day (Figure 7B).

4.2.2. Region 10: Bahia Blanca to Peninsula Valdés

In the region from Bahia Blanca to Peninsula Valdés, we reviewed 85 SLIPs and 31 limiting data points (Figure 7C). Only two types of paleo-sea level indicators are reported along these coasts: beach ridges (Codignotto et al., 1992) and marine terraces (Rostami et al., 2000). Most marine data points derive from sediment cores collected on the Argentine shelf (Guilderson et al., 2000).

In this region, as in Region 9, data from the Early Holocene is represented by limiting points (Supplementary Figure 2). The oldest SLIP (ID: 1147) places the sea level at 2.4 ± 2.3 m a.s l. around 7000 years cal BP. Since then, RSL values oscillate, ranging from 8.4 ± 2.3 m a.s.l. to -1.57 ± 1.2 m b.s.l. However, a general trend of an RSL fall after a Mid-Holocene highstand (6600 years cal BP) is observed. One SLIP (ID: 1164) shows the highest RSL value (12.4 ± 2.3 m

a.s.l.) around 5300 years cal BP (Figure 7C). However, this value seems at odds with the sea level trend during that time and this SLIP needs further examination.

The STEHM shows rising relative sea level, with rates up to 17.7 mm/yr, from ~9500 years cal BP to peak sea level at ~7000 years cal BP, followed by a gradual fall towards the present at an average rate of –0.2 mm/yr (Figure 7C, E). Comparing GIA models' predictions with the data, both models fit the data from 8000 cal BP to the present day (Figure 7C).

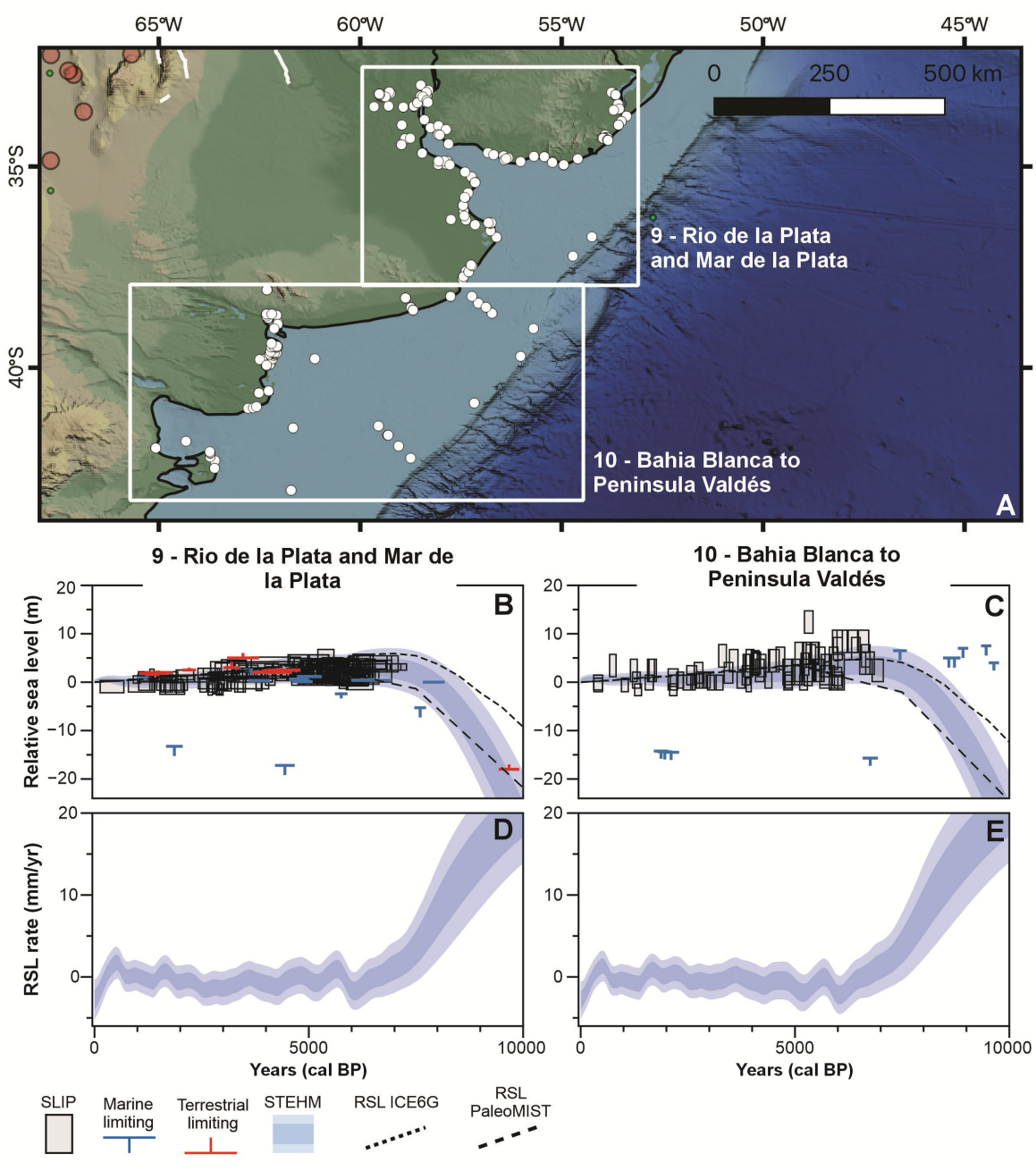

Figure 7. Map (A) and RSL reconstructions (B-E) and rates from regions 9 and 10 using the spatio-temporal model. For all plots, the model mean and 2σ uncertainty are represented by a solid line and shaded envelopes, respectively. Index points (grey boxes) are plotted as calibrated age against changes in sea level relative to the present. Limiting points are plotted as an "inverted-T" red symbol for terrestrial or an "T" blue symbol for marine. The dimensions of boxes and symbols for each point are based on elevation and age (2σ) errors. SLIP: sea-level index point; STEHM: spatio-temporal empirical hierarchical model; ICE6G (short, dashed line) and PaleoMIST (large, dashed line) represent the GIA models. Credits for the base map in A) are the same as Figure 1A.

4.2.3. Region 11: Bahia Vera to Puerto San Julián

The region from Bahia Vera to Puerto San Julián includes an extensive coastline from the center of Chubut Province to the south of Santa Cruz Province in Argentina. Here, we reviewed 132 SLIPs and 69 limiting data (Figure 8B). The most common indicators in the region are beach ridges (Codignotto et al., 1992; Schellmann, 2007; Schellmann and Radtke, 2010; Ribolini et al., 2011; Zanchetta et al., 2012; Zanchetta et al., 2014); although marine terraces (Rostami et al., 2000; Schellmann and Radtke, 2000; 2003; 2010; Schellmann, 2007), estuarine deposits (Bini et al., 2018), and one upper tidal flat (Desiage et al., 2023) are also described.

The records in Bahia Vera and Puerto San Julián date back to the Early Holocene (Supplementary Figure 2). The oldest SLIP (ID: 1444) places the RSL at -102 ± 0.7 m b.s.l. at ca. 13,200 years cal BP. Since then, the dataset shows scattered SLIPs with values ranging from 9 m a.s.l. to -1.0 m b.s.l. However, an RSL falling trend is observed (Figure 8B).

The STEHM, the RSL record shows a rising RSL from around 9000 years cal BP to approximately 7000 years cal BP, reaching a Mid-Holocene highstand at a mean rate of about 11.2 mm/yr. Following the highstand, the RSL gradually declined toward the present, with an average fall rate of roughly –0.4 mm/yr (Figure 8B, D). As in the previous region, both GIA models fit the data around 8000 cal BP (Figure 8B).

4.2.4. Region 12: Tierra del Fuego

In the southernmost Region, we reviewed 37 SLIPs and 62 limiting data (Figure 8C). The indicators described are beach ridges (Rabassa et al., 2000; Codignotto et al., 1992; Gordillo et al., 1993; Bujalesky, 2007; Isla and Bujalesky, 2008), marine terraces (Gordillo et al., 1993; Bujalesky, 2007; Isla and Bujalesky, 2008), beach deposits (Porter et al., 1984), basal peat (non-mangrove) (Porter et al., 1984; Gordillo et al., 1993; Bujalesky, 2007; Isla and Bujalesky, 2008), and lagoon deposits (Björck et al., 2021).

The SLIPs data mainly corresponds to the Mid-Holocene. However, some limiting data shows an Early Holocene age (Supplementary Figure 2). The oldest SLIP (ID:983) places the RSL at 1.9 ± 2.1 m b.s.l. ca. 6200 years cal BP. SLIPs between 5700 and 4400 years cal BP show variability in sea level between ~1.6 and ~4.6 m with peaks at 5700 (6.0 m) and 4400 (4.6 m). Overall, the data shows a general trend of sea level fall from the peak at about 5700 years (Figure 8C).

The STEHM shows a Mid-Holocene highstand occurring roughly between ~9000 and ~7000 years cal BP, with relative sea level rates peaking around 17.7 mm/yr. Following this highstand, the rates gradually decline from ~7000 years cal BP to the present, transitioning through near-zero values and eventually becoming negative, indicating a long-term relative sea level fall with rates reaching up to –3.3 mm/yr (Figure 8C, E). In this region, both GIA models fit the data since the Mid-Holocene (Figure 8C).

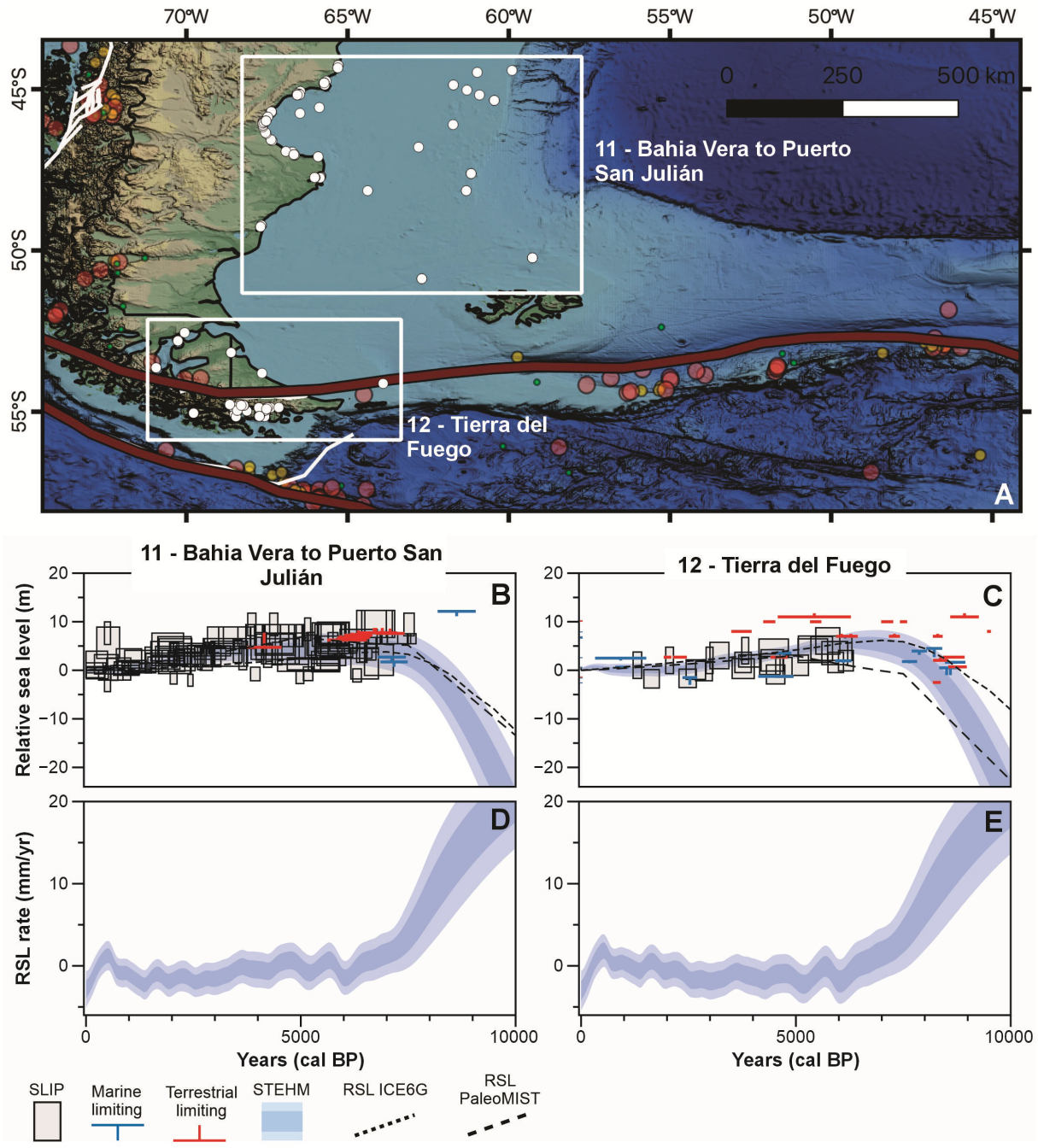

Figure 8. Map (A) and RSL reconstructions (B-E) and rates from regions 11, and 12 using the spatio-temporal model. For all plots, the model mean and 2σ uncertainty are represented by a solid line and shaded envelopes, respectively. Index points (grey boxes) are plotted as calibrated age against changes in sea level relative to the present. Limiting points are plotted as an "inverted-T" red symbol for terrestrial or an "T" blue symbol for marine. The dimensions of boxes and symbols for each point are based on elevation and age (2σ) errors. SLIP: sea-level index point; STEHM: spatio-temporal empirical hierarchical model; ICE6G (short, dashed line) and PaleoMIST (large, dashed line) represent the GIA models. Credits for the base map in A) are the same as Figure 1A.

5. Discussion

We developed a new standardized database of Holocene relative sea level (RSL) in the southwestern Atlantic, building on previous efforts by Milne et al. (2005) and Angulo et al. (2006). The database contains 1108 data points, including 701 sea-level index points (SLIPs), 100 terrestrial limiting points, and 307 marine limiting points. An additional 291 data points

were excluded due to missing information required by the standard protocols of the HOLSEA database (Khan et al., 2019).

5.1. Methodological Considerations in Building the RSL Database

Sea-level data were compiled from a diverse range of indicators, including beach deposits, sedimentary sequences, and fixed biological indicators. Our results show generally good agreement in RSL reconstructions derived from different indicators across most regions. However, in specific areas (regions 1 and 3), we observed that RSL estimates based on sedimentary sequences are up to ~1 m lower than those derived from other indicators. This discrepancy may be due to post-depositional lowering from compaction processes (Khan et al., 2022). Despite this inconsistency, our reconstructed RSL histories align well with previous compilations (e.g., Angulo et al., 2006; Milne et al., 2005; Figure 9A, B), further confirming that standardizing sea-level data can yield coherent results, even when different methods are used to quantify the indicative meaning of SLIPs.

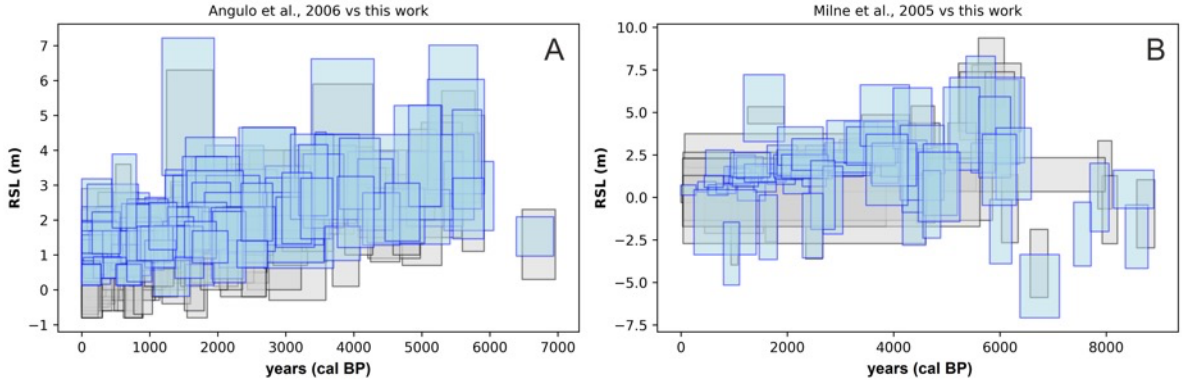

Figure 9. Comparison between our data (blue) and the standardized data of A) Angulo et al. (2006) and B) Milne et al. (2005) (grey).

In our database, vermetid rims from the Brazilian coast and beach ridges from Argentina and Uruguay constitute the majority of data points (e.g., Codignotto et al., 1992; Martin et al., 1996; Cavallotto, 2002; Angulo et al., 2006, 2022b; Bracco et al., 2011; Martínez and Rojas, 20013). We note that some sources of vertical error and uncertainty associated with these indicators—though not specifically addressed in this work—could affect the reported RSL interpretations. For example, Laborel (1986) notes that wave energy can shift the vertical distribution of vermetids by approximately 1 m. Angulo et al. (1999) identify three additional sources of uncertainty when using vermetid fossils to infer paleo-sea level: (i) the remains may not correspond to the upper limit of formation, (ii) the coastal hydrodynamic regime may have changed over time, and (iii) the vertical reference used to assess the displacement of vermetid reefs may be uncertain. Rovere et al. (2015) emphasize that most vermetid species have a broad living range, which can be narrowed when specific biological associations are considered (Angulo et al., 2022c). To standardize the vertical distribution and uncertainty of these indicators in our database, we adopted a general indicative range (MSL to MLLW) and defined an ad hoc datum (vermetid biological datum).

Paleo tidal range changes may also influence the indicative meaning of SLIPs whose vertical bounds are tied to tidal levels (e.g., Hill et al., 2011; Hall et al., 2013; Horton et al., 2013; Khan

et al., 2017; Sulzbach et al., 2023). For beach ridges, in this work, we follow the interpretation of Lorscheid and Rovere (2019) and Rovere et al. (2016), who suggest that they form above sea level, between the ordinary berm and the storm wave swash height, consistent with Tamura's (2012) definition of gravel beach ridges. According to this definition, mean higher high water (MHHW) is used to estimate both the ordinary berm and storm wave swash heights (Lorscheid and Rovere, 2019). Paleo tidal range changes may therefore be particularly relevant in areas with wide continental shelves, such as the Amazon River and Rio de la Plata deltas, and Bahia Blanca. In this study, we used satellite-derived wave measurements and wave runup models to calculate the indicative meaning of beach ridges, following the methodology of Rubio-Sandoval et al. (2024). While this approach does not fully resolve uncertainties related to paleo tidal ranges, it incorporates local wave and beach topography data and appears more reliable than the IMCalc software (Lorscheid and Rovere, 2019), which relies on global wave atlases and generalized beach slope values.

5.2. Holocene RSL variability along the southwestern Atlantic

We reconstructed Holocene RSL histories to capture local and regional sea-level variations over time along the southwestern Atlantic coastlines of Brazil, Uruguay, and Argentina (Figures 4, 5, 6, 7, and 8). In general, observed and predicted RSL changes show a rising trend between ~8000 and ~5000 years cal BP, with a mean rate of 1.7 mm/yr (Angulo and Lessa, 1997; Angulo et al., 2006; Schellmann and Radtke, 2010). This culminated in a highstand of ~2 to ~4 m above present sea level, followed by a gradual fall to modern levels. Given the broad spatial extent of the study area, this Mid- to Late Holocene trend is variably influenced by ice and ocean mass redistribution, and in some cases, by local crustal tectonics (Rostami et al., 2000; Milne et al., 2005).

In northern Brazil, estuarine deposits and mangroves from the Amazon River delta record a Mid-Holocene highstand of approximately 2 m above sea level. After this peak, RSL declined during the Late Holocene at a mean rate of 1.3 mm/yr (Figure 4D). This trend, excluding Atol das Rocas, differs from the rest of the northeastern sector. Regions from Pernambuco to northern Bahia show a highstand of approximately 5 m between ~6000 and ~4000 years cal BP, followed by a fall in RSL toward present levels (mean rate: –0.5 mm/yr). As noted by Angulo et al. (2006), SLIPs from mangrove swamp deposits in northern Brazil suggest a lower sea level than expected, indicating that neotectonics and wind-wave dynamics may influence the RSL trend in this area. Additionally, the effects of sedimentary compaction—which may alter sedimentary sea-level records by several meters (Hilma et al., 2015; Chelli et al., 2017)—should not be overlooked. Therefore, interpretations of sea-level trends in the Amazon delta estuarine region should be approached with caution, and further work is needed to quantify the role of compaction.

The scattered data in Atol das Rocas (Figure 6E) may reflect palaeoceanographic changes, which introduce vertical uncertainties in coral reef SLIPs (Shennan et al., 2018; Khan et al., 2019). As hydrodynamic conditions—such as waves, weather, and tides—affect the growth of coralline-algal reefs, these growth patterns may overlap with sea-level trends (Angulo et al., 2022a), leading to RSL histories that deviate from regional expectations.

In the region covering the Brazilian states from Sergipe to Bahia, a second sea-level peak is observed between ~4000 and ~2000 years cal BP (Figure 5). The presence of Late Holocene sea-level oscillations in Brazil has long been debated (Angulo and Lessa, 1997; Martin et al., 1998, 2003; Angulo et al., 2006). However, given the current data and associated uncertainties, we cannot propose a new interpretation, and more precise indicators are required to test the hypothesis of a second Holocene highstand and of Holocene sea-level oscillations.

The southeastern coastal sector of Brazil, from Espírito Santo to Santa Catarina, shows a coherent Holocene RSL trend (Figure 6). RSL rose rapidly from ~8000 years cal BP, reaching rates up to 7 mm/yr in some areas and averaging ~3 mm/yr overall. This sea-level rise culminated in a Mid-Holocene highstand between ~6000 and ~5000 years cal BP, with maximum RSL reaching ~3 to 4.7 m above present levels. Following this peak, RSL gradually declined at average rates up to ~0.3 mm/yr, reaching near-modern levels in the Late Holocene. These trends align with the global eustatic pattern described by Milne et al. (2005), who reported a rapid Early Holocene sea-level rise (~7–8 mm/yr) followed by deceleration. Moreover, the observed regional trends are consistent with GIA model predictions, particularly the ICE6G model, highlighting the importance of isostatic processes in shaping Holocene sea-level history in this sector.

Between the Río de la Plata delta and Tierra del Fuego, the Mid-Holocene highstand occurred slightly earlier (~7000 to ~6000 years cal BP) than in northern regions, and was similarly followed by a Late Holocene sea-level fall. However, highstand elevations vary across this extensive coastal stretch (Figures 7 and 8). Milne et al. (2005) proposed that this temporal offset results from the combined effect of West Antarctic ice sheet meltwater redistributing the geoid during the Early Holocene and from crustal subsidence in some parts of the region. They also note that various processes can cause vertical movement of both land and ocean surfaces, leading to a significant non-eustatic component of RSL change and, consequently, to variability in observed RSL values.

In addition to these differences in highstand elevation, the SLIP data between Río de la Plata and Tierra del Fuego are notably scattered (Figures 7 and 8). This may reflect differences in geomorphological settings, dating uncertainties, or limited spatial and temporal data coverage. Schellmann and Radtke (2010) suggest that discrepancies in RSL change along the Patagonian Atlantic coast may stem from gaps in geomorphological and chronostratigraphic records, compounded by variable ^{14}C reservoir effects that produce unquantifiable age uncertainties. We applied local Delta-R corrections where possible to reduce these errors; however, the lack of such correction data for Argentinean Patagonia limits interpretability, and these data should be treated cautiously.

In Tierra del Fuego, RSL reconstructions are likely shaped by a combination of chronological gaps (Schellmann and Radtke, 2010), GIA (Björck et al., 2021), and localized tectonic activity (Isla and Angulo, 2016; Rostami et al., 2000). Björck et al. (2021) argue that GIA, driven by the Patagonian Ice Sheet, is the dominant factor behind the elevated shorelines and the spatial–temporal variability of RSL in this area. In contrast, Rostami et al. (2000) contend that the Patagonian Ice Sheet—estimated to have a maximum thickness of ~400 m (Hulton et al., 1994)—would not have produced a significant RSL response along the Argentinean coast.

Their analysis shows that, contrary to expectations of forebulge collapse and sea-level rise, Holocene terraces in the region are uplifted rather than submerged, implying that localized tectonic uplift may have played a more important role. They estimate a consistent uplift rate of 0.09 m/1000 yr in Patagonia since the Mid-Pleistocene. Before a unique RSL history for this region can be established, limitations in both spatial and temporal data coverage—and an improved understanding of glacial history—must be addressed.

Despite the regional caveats discussed above, the influence of GIA across the broad latitudinal range covered by our database is evident in both the data and the STHEM model (Figures 4, 5, 6, 7, and 8). Generally, the Holocene highstand occurs later and with lower magnitude toward the north, following patterns predicted by GIA models. As shown by Peltier et al. (2015), highstand elevations in many locations can be reproduced by the ICE6G model, which incorporates rotational effects into sea-level calculations. The modified PaleoMIST model used in this study does not match data older than 5000 years cal BP, suggesting that global ice volume at ~7500 years cal BP may be overestimated by 4–5 m sea-level equivalent. The model's good performance after 5000 years cal BP supports the interpretation that Antarctic ice volume reached near-present levels by that time.

Although this study does not aim to extrapolate the revised Holocene sea-level curves to a broader regional scale, some comparisons are warranted. Despite uncertainties, the RSL reconstructions presented here align with expected trends for both near-field and far-field settings, with a few exceptions already discussed. The data from Tierra del Fuego, a near-field location due to its proximity to Antarctica, show a complex RSL fall following a highstand, shaped by the combined effects of eustatic rise and glacio-isostatic uplift (Milne and Mitrovica, 2007). In contrast, regions from the Río de la Plata delta (Uruguay) to the Amazon delta (Brazil) exhibit far-field RSL behavior. This latitudinal gradient supports the presence of a Mid-Holocene highstand (between ~8000 and ~4000 years cal BP) with elevations ranging from ~1 to 6 m (Kahn et al., 2015). Improving the quality of RSL data in this region, and integrating it with standardized datasets from intermediate-field areas (e.g., the Caribbean, Khan et al., 2017) and northern near-field sites (e.g., Atlantic USA, Englehart and Horton, 2012; Southern Maine, Kahn et al., 2015; Gulf of Maine, Baril et al., 2023; Canada, Vacchi et al., 2018; Greenland, Gowan et al., 2023), would support the development of a comprehensive pole-to-pole sea-level dataset. Such a resource would enhance GIA model calibration and improve estimates of global sea-level change since the Last Glacial Maximum.

6. Conclusions

We present the first standardized database of Holocene relative sea-level (RSL) indicators for the southwestern Atlantic, comprising over 1108 data points from Brazil, Uruguay, and Argentina. Despite the regional variability and occasional data gaps, our compilation reveals coherent RSL histories that highlight the interplay between glacio-isostatic adjustment (GIA), sediment compaction, and local tectonics across more than 50 degrees of latitude.

Our findings confirm a consistent Mid-Holocene highstand ranging from ~2 to ~6 meters above present sea level, followed by a gradual fall toward modern levels. This latitudinal gradient in highstand timing and magnitude aligns with GIA model predictions and underscores the region's value for testing and refining global sea-level models. The poor PaleoMIST model–

data agreement before 5000 years cal BP calls for revised estimates of global ice volume in Early Holocene scenarios in this model.

This work also underscores the importance of methodologically consistent approaches—especially in the treatment of complex indicators like vermetids and beach ridges—for generating reliable reconstructions. While challenges remain in underrepresented regions such as Patagonia and the Amazon delta, our database provides a robust foundation for future improvements.

Ultimately, this standardized RSL database bridges a critical gap in the global sea-level record. When combined with similar efforts in the Caribbean and higher-latitude regions, it will enable the development of integrated pole-to-pole sea-level reconstructions—an essential step toward enhancing GIA models and constraining global sea-level budgets since the Last Glacial Maximum.

Data availability

The database is available at https://doi.org/10.5281/zenodo.10819555 (Version 2.0; Rubio-Sandoval et al., 2025). Any modification to the database can be requested through the platform WALIS (https://warmcoasts.eu/walis/Data_mod_request_open/).

Acknowledgments

This work is part of the PhD thesis of Karla Rubio-Sandoval, funded by the European Research Council (ERC) under the European Union's Horizon 2020 research and innovation program (grant agreement no. 802414). Karla Rubio-Sandoval also acknowledges the Monika Segl program of MARUM, Bremen University, for additional support. She also thanks the Instituto de Geociencias and DGAPA (Dirección General de Asuntos del Personal Académico) for the postdoctoral fellowship that was essential to complete the publication of this work. Timothy Adam Shaw and Ben Horton were supported by the Singapore Ministry of Education Academic Research Fund MOE2019-T3-1 004, the National Research Foundation Singapore, the Singapore Ministry of Education under the Research Centers of Excellence initiative, and by the Nanyang Technological University. This work is Earth Observatory of Singapore contribution number XXX. We would like to thank Abdulla S. Khan for technical support during the development of the database and Lic. Ricardo Briseño López for his guidance in the design of the illustrations. We thank to the PALSEA working group for the useful discussions during the 2022 meeting in Singapore. PALSEA is a working group of the International Union for Quaternary Sciences (INQUA) and Past Global Changes (PAGES), which in turn received support from the Swiss Academy of Sciences and the Chinese Academy of Sciences. Figure 1 weas created using ArcGIS® software by Esri. ArcGIS® and ArcMap™ are the intellectual property of Esri and are used herein under license © Esri. All rights reserved. For more information about Esri® software, please visit https: //www.esri.com (last access: 20.06.2023). The data used in this study were compiled in WALIS, a sea-level database interface developed by the ERC Starting Grant WARMCOASTS (ERC-StG-802414) in collaboration with the PALSEA working group. The database structure was designed by Alessio Rovere, Deirdre D. Ryan, Thomas Lorscheid, Andrea Dutton, Peter Chutcharavan, Dominik Brill, Nathan Jankowski, Daniela Mueller, Melanie Bartz, Evan Gowan, and Kim Cohen. The beta-version of the WALIS

data insertion interface for Holocene sea-level data was coded thanks to partial support by a PAGES Data Stewardship Scholarship. The authors used ChatGPT (OpenAI) to improve the clarity and readability of some paragraphs in the Discussion section. The authors reviewed and verified all content to ensure accuracy and scientific integrity.

References

Aguirre, M.L., 1993. Palaeobiogeography of the Holocene molluscan fauna from Northeastern Buenos Aires Province, Argentina: its relation to coastal evolution and sea level changes. Palaeogeogr Palaeoclimatol Palaeoecol 102, 1–26.

Albero, M.C., Angiolini, F.E., 1983. Ingeis Radiocarbon Laboratory Dates. Radiocarbon 831–842.

Amato, S., Busso, A.S., 2009. Estratigrafía Cuaternaria del subsuelo de la cuenca inferior del Río Paraná, Revista de la Asociación Geológica Argentina.

Angulo, R.J., 1992. Ambientes de sedimentação planície costeira com cordões litorâneos no estado do Paraná. Boletin Paranaense de Geociências 40, 69–114.

Angulo, R.J., 1989. Fossil vermetidae between latitudes 25° 34´ S and 27° 09´S state of Paraná and state of Santa Catarina- Brazil. International symposium on global changes in South America during the Quaternary: Past- Present- Future 263–268.

Angulo, R.J., Camargo Lessa, G., 1997. The Brazilian sea-level curves: a critical review with emphasis on the curves from the ParanaguA and Canan&a regions, Marine Geology.

Angulo, R. J., de Souza, M. C., 2014. Conceptual review of Quaternary coastal paleo-sea level indicators from Brazilian coast. Quaternary and Environmental Geosciences, 5(2), 01 32.

Angulo, R.J., de Souza, M.C., da Camara Rosa, M.L.C., Barboza, E.G., Lessa, G.C., Pessenda, L.C.R., Ferreira Junior, A.L., 2022b. Mid- to Late Holocene sealevel changes at Abrolhos Archipelago and Bank, southwestern Atlantic, Brazil. Mar Geol 450. https://doi.org/10.1016/j.margeo.2022.106841

Angulo, R.J., de Souza, M.C., da Camara Rosa, M.L.C., Caron, F., Barboza, E.G., Costa, M.B.S.F., Macedo, E., Vital, H., Gomes, M.P., Garcia, K.B.L., 2022a. Paleo-sea levels, Late-Holocene evolution, and a new interpretation of the boulders at the Rocas Atoll, southwestern Equatorial Atlantic. Mar Geol 447. https://doi.org/10.1016/j.margeo.2022.106780

Angulo, R. J., de Souza, M. C., Giannini, P. C. F., Dillenburg, S. R., Barboza, E. G., da Camara Rosa, M. L. C., Hesp, P.A., Pessenda, L. C. R., 2022c. Late-Holocene sea levels from vermetids and barnacles at Ponta do Papagaio, 27° 50' S latitude and a comparison with other sectors of southern Brazil. Quaternary Science Reviews, 286, 107536.

Angulo, R.J., Giannini, P.C.F., De Souza, M.C., Lessa, G.C., 2016. Holocene paleo-sea level changes along the coast of Rio de Janeiro, southern Brazil: Comment on Castro et al. (2014). An Acad Bras Cienc 88, 2105–2111. https://doi.org/10.1590/0001-3765201620140641

Angulo, R.J., Giannini, P.C.F., Souza, M.C., Lessa, G.C., 2018. Reply to Castro et al. 2018 on "Holocene paleo-sea level changes along the coast of Rio de Janeiro, southern Brazil". An Acad Bras Cienc 90, 1377–1380. https://doi.org/10.1590/0001-3765201820180376

Angulo, R.J., Giannini, P.C.F., Suguio, K., Pessenda, L.C.R., 1999. Relative sea-level changes in the last 5500 years in southern ž / Brazil Laguna-Imbituba region, Santa Catarina State based on vermetid 14 C ages, Marine Geology.

Angulo, R.J., Lessa, G.C., de Souza, M. c, 2006. A critical review of mid-to late-Holocene sea-level fluctuations on the eastern Brazilian coastline. Quat Sci Rev 25, 486–506.

Argus, D.F., Peltier, W.R., Drummond, R., Moore, A.W., 2014. The Antarctica component of postglacial rebound model ICE-6G_C (VM5a) based upon GPS positioning, exposure age dating of ice thicknesses, and relative sea level histories. Geophys. J. Int., 198(1), 537-563,

Angulo, R.J., Pessenda, L., Souza, M.C., 2002. O significado das datações ao 14C na reconstrução de paleoníveismarinhos e na evolução das barreiras Quaternárias do litoral paranaense. Revista Brasileira de Geociências 32, 95–106.

Ashe, E. L., Cahill, N., Hay, C., Khan, N. S., Kemp, A., Engelhart, S. E., Benjamin, P.H, Parnell, A.C., Kopp, R. E., 2019. Statistical modeling of rates and trends in Holocene relative sea level. Quaternary Science Reviews, 204, 58-77.

Babtista de Jesus, P., Dias, F. F., Muniz, R. D. A., Macário, K. C. D., Seoane, C. S., Quattrociocchi, D. G. S., Tardin, R.C., Aguilera, O., Correa, R.C., Queiroz, E., Silva, I., Alves, C.R., Araujo, J. C., 2017. Holocene paleo-sea level in southeastern Brazil: an approach based on vermetids shells. Journal of Sedimentary Environments, 2(1), 35-48.

Backeuser E., 1918. A faixa litorânea do Brasil Meridional. Ontem ehoje. Tyy. Besnard Frêres, Rio de Janeiro. 207p.

Barbosa, L.M., Bittencourt, A.C.D.A., Dominguez, J.M., Martin, L., 1986. The Quaternary coastal deposits of the State of Alagoas: influence of the relative sea-level changes, in: Quaternary of South America and Antarctic Peninsula. pp. 269–290.

Baril, A., Garrett, E., Milne, G. A., Gehrels, W. R., Kelley, J. T. 2023. Postglacial relative sea-level changes in the Gulf of Maine, USA: Database compilation, assessment and modelling. Quaternary Science Reviews, 306, 108027.

Barreto, A.M.F., Bezerra, F.H.R., Suguio, K., Tatumi, S.H., Yee, M., Paiva, R.P., Munita, C.S., 2002. Late Pleistocene marine terrace deposits in northeastern Brazil: sea-level change and tectonic implications. Paleogeography, Paleoclimatology, Paleoecology 179, 57–69.

Behling, H., Cohen, M.C.L., Lara, R.J., 2004. Late Holocene mangrove dynamics of Marajó Island in Amazonia, northern Brazil. Veg Hist Archaeobot 13, 73–80. https://doi.org/10.1007/s00334-004-0031-1

Behling, H., Cohen, M.C.L., Lara, R.J., 2001. Studies on Holocene mangrove ecosystem dynamics of the Bragança Peninsula in north-eastern Pará, Brazil. Palaeogeography, Palaeockimatology, Palaeoecology 167, 225–242.

867 Bernal, J.P., Beramedi, L.E., Lugo-Ibarra, K.C., Walter, L., 2010. Revisión a algunos
868 geocronómetros radiométricos aplicables al Cuaternario. Boletín de la Sociedad Geológica
869 Méxicana 62, 305–323.

870 Bezerra, F.H.R., Vita-Finzi, C., 2000. How active is a passive margin? Paleoseismicity in
871 northeastern Brazil. Geology 591–595.

872 Bini, M., Isola, I., Zanchetta, G., Pappalardo, M., Ribolini, A., Ragaini, L., Baroni, C., Boretto, G.,
873 Fuck, E., Morigi, C., Salvatore, M.C., Bassi, D., Marzaioli, F., Terrasi, F., 2018. Mid-Holocene
874 relative sea-level changes along Atlantic Patagonia: New data from Camarones, Chubut,
875 Argentina. Holocene 28, 56–64. https://doi.org/10.1177/0959683617714596

876 Bird, P. (2003). An updated digital model of plate boundaries. Geochemistry, Geophysics,
877 Geosystems, 4(3).

878 Bittencourt, A.D.S., Martin, L., Vilas Boas, G.D.S., Flexor, J.M., 1978. Quaternary marine
879 formations of the coast of the state of Bahia (Brazil), in: Proceedings of 1978 International
880 Symposium on Coastal Evolution in the Quaternary, 232–253.

881 Björck, S., Lambeck, K., Möller, P., Waldmann, N., Bennike, O., Jiang, H., Li, D., Sandgren, P.,
882 Nielsen, A.B., Porter, C.T., 2021. Relative sea level changes and glacio-isostatic modelling in
883 the Beagle Channel, Tierra del Fuego, Chile: Glacial and tectonic implications. Quaternary
884 Science Reviews, 251, 106-657.

885 Bracco, R., 1991 Dataciones 14C en Sitios con Elevación. Rev. Antropología, año 1, *I*: 11-17.

886 Bracco, R., 2000. Aproximación al registro arqueológico del sitio La Esmeralda ("conchero")
887 desde su dimensión temporal. Anales de Arqueología y Etnología 54–55.

888 Bracco, R., García-Rodríguez, F., Inda, H., del Puerto, L., Castiñeira, c, Penario, D., 2011. Niveles
889 relativos del mar durante el Pleistoceno final-Holoceno en la costa de Uruguay, in: El
890 Holoceno En La Zona Costera de Uruguay. pp. 65–92.

891 Bracco, R., Inda, H., del Puerto, L., Capdepont, I., Panario, D., Castiñeira, C., García-Rodríguez,
892 F., 2014. A reply to "Relative sea level during the Holocene in Uruguay." Palaeogeogr
893 Palaeoclimatol Palaeoecol.

894 Bracco, R., Ures, M.C., 1998. Las variaciones del nivel del mar y el desarrollo de las culturas
895 prehistóricas del Uruguay. Revista do Museu de Arqueologia e Etnologia, (8), 109-115.

896 Branner J.C, 1889. The geology of Fernando de Noronha. American Journal of Science. 37:145-
897 161.

898 Branner J.C., 1890. The aeolian sandstones of Fernando de Noronha. American Journal of
899 Science. 39:247-257.

900 Branner J.C., 1902. Geology of northeast coast of Brazil. Bulletin of the Geological Society of
901 America, 13:41-98.

902 Branner J.C., 1904. The stone reef of Brazil, their geological and geographical relations, with a
903 chapter on the coral reefs. Bulletin of the Museum of Comparative Zoology at Harvard
904 College v. 44, Geological Series v. 7. Cambridge, Massachuset, U.S.A. 285p. 99

Bujalesky, 2007. Coastal geomorphology and evolution of Tierra del Fuego (Southern Argentina).

Carrere, L., Lyard, F., Cancet, M., Guillot, A., Picot, N., 2016. Fes2014, a new tidal model–validation results and perspectives for improvements, presentation to esa living planet conference.

Castro, A., Wagner, J., Sicoli, S., Fernandes, D., Cabral, C., Meneguci da Cunha, A., Malta, J., Miguel, L., Areia de Oliveira, C., Spotorno de Oliveira, P., Tapajós de Souza Tamega, F., 2021. Relative sea-level curve during the Holocene in Rio de Janeiro, Southeastern Brazil: A review of the indicators - RSL, altimetric and geochronological data. J South Am Earth Sci 112. https://doi.org/10.1016/j.jsames.2021.103619

Castro, J.W.A., Seoane, J.C.S., Cunha, A.M., Malta, J. V., Oliveira, C.A., VAZ, S.R., Suguio, K., 2018. Comments to Angulo et al. 2016 on "Sea-level fluctuations and coastal evolution in the state of Rio de Janeiro, southeastern - Brazil" by Castro et al. 2014. An Acad Bras Cienc 90, 1369–1375. https://doi.org/10.1590/0001-3765201820171010

Castro, J.W.A., Suguio, K., Seoane, J.C.S., Da Cunha, A.M., Dias, F.F., 2014. Sea-level fluctuations and coastal evolution in the state of Rio de Janeiro, southeastern Brazil. An Acad Bras Cienc 86, 671–683. https://doi.org/10.1590/0001-3765201420140007

Cavallotto, J.L., 2002. Evolución holocena de la llanura costera del margen sur del Río de la Plata. Rev. Asoc. Geol. Argent 57, 376–388.

Cavallotto, J.L., 1995. Evolución geomorfológica de la llanura costera ubicada en el margen sur del Río de la Plata. Universidad Nacional de La Plata.

Cavallotto, J.L., Violante, R.A., Colombo, F., 2005. Evolución y cambios ambientales de la llanura costera de la cabecera del río de la Plata.

Cavallotto, J.L., Violante, R.A., Parker, G., 2004. Sea-level fluctuations during the last 8600 years in the de la Plata river (Argentina). Quaternary International 114, 155–165. https://doi.org/10.1016/S1040-6182(03)00050-8

Chelli, A., Pappalardo, M., Bini, M., Brückner, H., Neri, G., Neri, M., Spada, G. 2017. Assessing tectonic subsidence from estimates of Holocene relative sea-level change: An example from the NW Mediterranean (Magra Plain, Italy). The Holocene, 27(12), 1988-1999.

Codignotto, J.O., Kokot, R.R., Marcomini, S.C., 1992. Neotectonism and Sea-Level Changes in the Coastal Zone of Argentina, Source: Journal of Coastal Research.

Cohen, M.C.L., Behling, H., Lara, R.J., 2005. Amazonian mangrove dynamics during the last millennium: The relative sea-level and the Little Ice Age. Rev Palaeobot Palynol 136, 93–108. https://doi.org/10.1016/j.revpalbo.2005.05.002

Cohen, M. C., Figueiredo, B. L., Oliveira, N. N., Fontes, N. A., França, M. C., Pessenda, L. C., de Souza, A.V., Macario, K., Guiannini, P.C.F., Bendassolli, J.A., Lima, P., 2020. Impacts of Holocene and modern sea-level changes on estuarine mangroves from northeastern Brazil. *Earth Surface Processes and Landforms*, *45*(2), 375-392.

Cohen, M.C.L., Pessenda, L.C.R., Behling, H., de Fátima Rossetti, D., França, M.C., Guimarães, J.T.F., Friaes, Y., Smith, C.B., 2012. Holocene palaeoenvironmental history of the Amazonian mangrove belt. Quat Sci Rev 55, 50–58. https://doi.org/10.1016/j.quascirev.2012.08.019

Colado, U., Figini, A., Fidalgo, F., Fucks, E., 1995. Los depósitos marinos del Cenozoico Superior aflorantes en la zona comprendida entre Punta Indio y el río Samborombón, provincia de Buenos Aires.

Cortelezzi, C.R., 1977. Datacion de las formaciones marinas en el Cuaternario en las proximidades de la Plata-Magdalena, Providencia de Buenos Aires. Anales del Laboratorio de Ensayo de Materiales e Investigaciones Tecnológicas 75–93.

Cortelezzi, C.R., Pavlicelic, R.E., Pitori, C.A., Parodi, A.V., 1992. Variaciones del nivel del mar en el Holoceno en los alrededores de La Plata y Berisso. Actas. IV Reunión Argentina de Sedimentología, La Plata 2, 131–138.

Darwin, C., 1851. *Geological observations on coral reefs, volcanic islands, and on South America: Being the geology of the voyage of the Beagle, under the command of Captain Fitzroy, RN, during the years 1832 to 1836*. Smith, Elder.

de Boer, B., Stocchi, P., Van De Wal, R. 2014. A fully coupled 3-D ice-sheet-sea-level model: algorithm and applications. Geoscientific Model Development 7, 2141–2156.

de Boer, B., Stocchi, P., Whitehouse, P.L., van de Wal, R.S. 2017. Current state and future perspectives on coupled ice-sheet – sea-level modelling. Quaternary Science Reviews 169, 13–28.

Delibrias, C., Laborel, J., 1971. Recent variations of the sea level along the Brazilian Coast. Quaternaria 45–49.

Desiage, P. A., St-Onge, G., Duchesne, M. J., Montero-Serrano, J. C., Haller, M. J., 2023. Late Pleistocene and Holocene transgression inferred from the sediments of the Gulf of San Jorge, central Patagonia, Argentina. Journal of Quaternary Science, 38(5), 629-646.

Dominguez, J.M.L., Bittencourt, A.C.S.P., Leão, Z.M.A.N., Azevedo, A.E.G., 1990. Geologia do Quaternário costeiro do estado de Pernanbuco. Revista Brasileira de Geociências 20.

Düsterhus, A., Rovere, A., Carlson, A.E., Horton, B.P., Klemann, V., Tarasov, L., Barlow, N.L.M., Bradwell, T., Clark, J., Dutton, A., Roland Gehrels, W., Hibbert, F.D., Hijma, M.P., Khan, N., Kopp, R.E., Sivan, D., Törnqvist, T.E., 2016. Palaeo-sea-level and palaeo-ice-sheet databases: Problems, strategies, and perspectives. Climate of the Past 12, 911–921. https://doi.org/10.5194/cp-12-911-2016

Engelhart, S.E., Horton, B.P., 2012. Holocene sea level database for the Atlantic coast of the United States. Quat. Sci. Rev. 54, 12e25. https://doi.org/10.1016/j.quascirev.2011.09.013.

Fasano, J., Ilsa, F., Schnack, E., 1983. Un análisis comparativo sobre la evolución de ambientes litorales durante el Pleistoceno tardío-Holoceno: Laguna Mar Chiquita (Buenos Aires) - Caleta Valdes (Chubut). In Simposio" Oscilaciones del nivel del mar durante el ultimo hemiciclo deglacial en la Argentina". CONICET, CAPICG, IGCP 61, 27–47.

Figini, A., 1992. Edades 14C de sedimentos marinos holocénicos de la provincia de Buenos Aires. Actas de las Terceras Jornadas Geológicas Bonaerenses 1, 147–151.

Flexor, J.M., Martin, L., 1979. Sur l´utilisation des gres coquilliers de la region de Salvador (Bresil) dans la reconstruction des lignes de rivages Holocenes. Proceedings of the "1978 International symposium on coastal evolution in the Quaternary" 343–355.

Fontes, N.A., Moraes, C.A., Cohen, M.C.L., Alves, I.C.C., França, M.C., Pessenda, L.C.R., Francisquini, M.I., Bendassolli, J.A., Macario, K., Mayle, F., 2017. The impacts of the middle holocene high Sea-Level stand and climatic changes on mangroves of the jucuruÇu river, southern Bahia-Northeastern Brazil. Radiocarbon 59, 215–230. https://doi.org/10.1017/RDC.2017.6

Fucks, E., De Francesco, F.O., 2003. Ingresiones marinas al norte de la ciudad de Buenos Aires. Su Ordenamiento Estratigráfico. Actas 2º Congreso Argentino de Cuaternario y Geomorfología 101-103.

Garrett, E., Melnick, D., Dura, T., Cisternas, M., Ely, L. L., Wesson, R. L., Jara-Muñoz, J., Whitehouse, P. L., 2020. Holocene relative sea-level change along the tectonically active Chilean coast. Quaternary Science Reviews, 236, 106281.

Gherardi, D.F.M., Bosence, D.W.J., 2005. Late Holocene reef growth and relative sea-level changes in Atol das Rocas, equatorial South Atlantic. Coral Reefs 24, 264–272. https://doi.org/10.1007/s00338-005-0475-5.

González, M.A., Ravizza, G., 1987. Sedimentos estuáricos del Pleistoceno tardío y Holoceno en la isla Martín García, río de la Plata. Revista Asociación Geológica Argentina 42, 231–243.

Gordillo, S., Coronato, A.M.J., Rabassa, J.O., 1993. Late Quaternary evolution of a Subantarctic Paleofjord, Tierra del fuego, Science Reviews.

Gowan., 2023. Comparison of the PaleoMIST 1.0 ice sheet margins, ice sheet and paleo-topography reconstruction with paleo sea level indicators (2.0). Zenodo. https://doi.org/10.5281/zenodo.7923553

Gowan, E.J., Rovere, A., Ryan, D.D., Richiano, S., Montes, A., Pappalardo, M., Aguirre, M.L., 2021a. Last interglacial (MIS 5e) sea-level proxies in southeastern South America. Earth Syst Sci Data 13, 171–197. https://doi.org/10.5194/essd-13-171-2021.

Gowan, E. J. 2023. Paleo sea-level indicators and proxies from Greenland in the GAPSLIP database and comparison with modelled sea level from the PaleoMIST ice-sheet reconstruction. *GEUS Bulletin*, *53*. https://doi.org/10.34194/geusb.v53.8355

Gowan, E.J., Zhang, X., Khosravi, S., Rovere, A., Stocchi, P., Hughes, A.L.C., Gyllencreutz, R., Mangerud, J., Svendsen, J., Lohmann, G., 2021b. A new global ice sheet reconstruction for the past 80 000 years. Nature Communications 12, 1199.

Guida, N., González, M.A., 1984. Evidencias paleoestuáricas en el sudeste de Entre Ríos, su evolución con niveles marinos relativamente elevados del Pleistoceno Superior y Holoceno.

1018 Guilderson, T. P., Burckle, L., Hemming, S., Peltier, W. R., 2000. Late Pleistocene sea level
1019 variations derived from the Argentine Shelf. Geochemistry, Geophysics, Geosystems, 1(12).

1020 Guimarães, J.T.F., Cohen, M.C.L., Pessenda, L.C.R., França, M.C., Smith, C.B., Nogueira, A.C.R.,
1021 2012. Mid- and late-Holocene sedimentary process and palaeovegetation changes near the
1022 mouth of the Amazon River. Holocene 22, 359–370.
1023 https://doi.org/10.1177/0959683611423693

1024 Hall, G.F., Hill, D.F., Horton, B.P., Engelhart, S.E., Peltier, W.R., 2013. A high-resolution study
1025 of tides in the Delaware Bay: Past conditions and future scenarios. Geophys Res Lett 40,
1026 338–342. https://doi.org/10.1029/2012GL054675

1027 Hartt C. F.,1870. Geology and physical geography of Brazil. Fields, Osgood & Co., Boston, 620p.

1028 Heaton, T.J., Köhler, P., Butzin, M., Bard, E., Reimer, R.W., Austin, W.E.N., Bronk Ramsey, C.,
1029 Grootes, P.M., Hughen, K.A., Kromer, B., Reimer, P.J., Adkins, J., Burke, A., Cook, M.S.,
1030 Olsen, J., Skinner, L.C., 2020. Marine20 - The Marine Radiocarbon Age Calibration Curve (0-
1031 55,000 cal BP). Radiocarbon 62, 779–820. https://doi.org/10.1017/RDC.2020.68

1032 Hijma, M.P., Engelhart, S.E., Törnqvist, T.E., Horton, B.P., Hu, P., Hill, D.F., 2015. A protocol for
1033 a geological sea-level database, in: Handbook of Sea-Level Research. Wiley Blackwell, pp.
1034 536–553. https://doi.org/10.1002/9781118452547.ch34

1035 Hill, D.F., Griffiths, S.D., Peltier, W.R., Horton, B.P., Törnqvist, T.E., 2011. High-resolution
1036 numerical modeling of tides in the western Atlantic, Gulf of Mexico, and Caribbean Sea
1037 during the Holocene. J Geophys Res Oceans 116. https://doi.org/10.1029/2010JC006896

1038 Hogg, A. G., Heaton, T. J., Hua, Q., Palmer, J. G., Turney, C. S., Southon, J., Bayliss, A., Blackwell,
1039 P.G., Boswijk, G., Ramsey, C.B., Pearson, C., Petchey, F., Reimer, P., Reimer, R., Wacker, L.
1040 (2020). SHCal20 Southern Hemisphere calibration, 0–55,000 years cal BP. Radiocarbon,
1041 62(4), 759-778.

1042 Horton, B.P., Engelhart, S.E., Hill, D.F., Kemp, A.C., Nikitina, D., Miller, K.G., Peltier, W.R., 2013.
1043 Influence of tidal-range change and sediment compaction on Holocene relative sea-level
1044 change in New Jersey, USA. J Quat Sci 28, 403–411. https://doi.org/10.1002/jqs.2634

1045 Horton, B.P., Kopp, R.E., Garner, A.J., Hay, C.C., Khan, N.S., Roy, K., Shaw, T.A., 2018. Annual
1046 Review of Environment and Resources Mapping Sea-Level Change in Time, Space, and
1047 Probability. https://doi.org/10.1146/annurev-environ

1048 Hu, P., 2010. Developing a Quality-controlled Postglacial Sea-level Database for Coastal
1049 Louisiana to Assess Conflicting Hypotheses of Gulf Coast Sea-level Change (MSc Thesis).
1050 Tulane University, New Orleans.

1051 Hulton, N., Sugden, D., Payne, A., Clapperton, C., 1994. Glacier modelling and the climate of
1052 Patagonia during the Last Glacial Maximum. Quaternary Research 42, 1-19.

1053 Isla, F.I., Angulo, R.J., 2016. Tectonic Processes along the South America Coastline Derived
1054 from Quaternary Marine Terraces. J Coast Res 32, 840–852.
1055 https://doi.org/10.2112/JCOASTRES-D-14-00178.1

Isla, F.I., Bujalesky, G.G., 2008. Coastal Geology and Morphology of Patagonia and the Fuegian Archipelago. Developments in Quaternary Science. https://doi.org/10.1016/S1571-0866(07)10010-5

Khan, N.S., Ashe, E., Horton, B.P., Dutton, A., Kopp, R.E., Brocard, G., Engelhart, S.E., Hill, D.F., Peltier, W.R., Vane, C.H., Scatena, F.N., 2017. Drivers of Holocene sea-level change in the Caribbean. Quat Sci Rev. https://doi.org/10.1016/j.quascirev.2016.08.032

Khan, N. S., Ashe, E., Moyer, R. P., Kemp, A. C., Engelhart, S. E., Brain, M. J., Toth, L.T., Chappel, A. Christie, M., Kopp, R.E, Horton, B. P., 2022. Relative sea-level change in South Florida during the past~ 5000 years. Global and Planetary Change, 216, 103902.

Khan, N.S., Ashe, E., Shaw, T.A., Vacchi, M., Walker, J., Peltier, W.R., Kopp, R.E., Horton, B.P., 2015. Holocene Relative Sea-Level Changes from Near-, Intermediate-, and Far-Field Locations. Curr Clim Change Rep 1, 247–262. https://doi.org/10.1007/s40641-015-0029-z

Khan, N.S., Horton, B.P., Engelhart, S., Rovere, A., Vacchi, M., Ashe, E.L., Törnqvist, T.E., Dutton, A., Hijma, M.P., Shennan, I., 2019. Inception of a global atlas of sea levels since the Last Glacial Maximum. Quat Sci Rev 220, 359–371. https://doi.org/10.1016/j.quascirev.2019.07.016

Kikuchi, R., Leao, Z., 1997. Rocas (Southwestern Equatorial Atlantic, Brazil): An atoll built primarily by coralline algae. Proc 8th Int Coral Reef Sym 1, 731–736.

Laborel, J., 1969. Les peuplements de Madréporaires des côtes tropicales du Brésil. Annales de l'Université d'Abidjan 2.

Laborel, J. 1986. Vermetid gastropods as sea-level indicators. *In Sea-level research: a manual for the collection and evaluation of data* (pp. 281-310). Dordrecht: Springer Netherlands.

Leaman, C., Beuzen, T., Goldstein E. B., 2020. Chrisleaman/py-wave-runup: v0.1.10

Lorscheid, T., Rovere, A., 2019. The indicative meaning calculator – quantification of paleo sea-level relationships by using global wave and tide datasets. Open Geospatial Data, Software and Standards 4. https://doi.org/10.1186/s40965-019-0069-8

Lyard, F. H., Allain, D. J., Cancet, M., Carrère, L., Picot N., 2021. Fes2014 global ocean tide atlas: design and performance. Ocean Science 17(3), 615–649.

Macario, K. D., Alves, E. Q., Oliveira, F. M., Scheel-Ybert, R., Dias, F. F., Lima, G. M.,2023. The variable nature of the coastal 14C marine reservoir effect: A temporal perspective for Rio de Janeiro. Quaternary Science Advances, 11, 100086.

Martínez, S.A., Rojas, A., Verde, M., Piñeiro, G., 2006. Molluscan assemblages from the marine Holocene of Uruguay: Composition, geochronology, and paleoenvironmental signals Palaeontology and Palaeoenvironments of continental invertebrates from Argentina View project Origin and evolution of the NW Pacific Cenozoic sand dollar fauna View project.

Martínez, S., Rojas, A., 2013. Relative sea level during the Holocene in Uruguay. Palaeogeogr Palaeoclimatol Palaeoecol 374, 123–131. https://doi.org/10.1016/j.palaeo.2013.01.010

Martin, L., Bittencourt, A. C. S. P., Dominguez, J. M. L., Flexor, J. M., Suguio, K. 1998 Oscillations or not oscillations, that is the question: Comment on Angulo, RJ and Lessa, GC ‘‘The Brazilian sea-level curves: a critical review with emphasis on the curves from the Paranagua’and Cananeia regions [Mar. Geol. 140,141–166]. Marine Geology, 150, 179-187.

Martin, L., Bittencourt, A.C.S.P., Vilas Boas, G.S., 1982. Primeira ocorrência de corais pleistocênicos na costa brasileira- Datação do máximo da Penúltima Transgressão.

Martin, L., Dominguez, J. M., Bittencourt, A. C. 2003. Fluctuating Holocene sea levels in eastern and southeastern Brazil: evidence from multiple fossil and geometric indicators. *Journal of Coastal Research*, 101-124.

Martin, L.K., Suguio, J.M., Flexor, J., Dominguez, M.L., Bittencourt, A.C.S.P., 1996. Quaternary sea-level history along the central Part of the Brazilian Coast. Variations in coastal dynamics and their consequences on coastal plain construction. An.Acad.bras.Ci. 68, 303–354.

Martin, L., Sugion, K., Flexor, J.M., Bittencourt, A.C.S.P., Vilas-Boas, G.S., 1979. Le quaternaire marin bresilien (littoral pauliste, sud fluminese et bahianais). Serie Geologie 11, 95–124.

Martin, L., Suguio, K., 1989. Excursion route along the Brazilian coast between Santos (state of São Paulo) and Campos (state of Rio de Janeiro). International Symposium on Global Changes in South America during the Quaternary 2.

Martin, L., Suguio, K., 1978. Excursionroute along the coastline between the town of Cananéisa (state of São Paulo) and Guaratiba outlet (state Rio de Janeiro), in: Internarional Symposium on Coastal Evolution . pp. 1–98.

Martin, L., Suguio, K., 1975.Étude préliminaire du Quaternaire Marin: comparaison du litroral de Sao-Paulo et de Salvador de Bahia (Brésil). Cah.O.R.S.T.O.M. 8, 33–47.

Martin, L., Suguio, K., Dominguez, J.M.L., Flexor, J.M., 1997. Geologia do Quaternário Costeiro do Litoral Norte do Rio de Janeiro e do Espirito Santo. Belo Horizonte: CPRM Servico Geologico do Brasil.

Martin, L., Flexor, J. M., Blitzkow, D., Suguio, K. 1985. Geoid change indications along the Brazilian coast during the last 7.000 years. In *Proceedings*

Mauz, B., Vacchi, M., Green, A., Hoffmann, G., Cooper, A., 2015. Beachrock: A tool for reconstructing relative sea level in the far-field. Mar Geol 362, 1–16. https://doi.org/10.1016/j.margeo.2015.01.009

McHutchon, A., Rasmussen, C.E., 2011. Gaussian Process Training with Input Noise. In: Shawe-Taylor, J., Zemel, R.S., Bartlett, P.L., Pereira, F., Weinberger, K.Q. (Eds.), Advances in Neural Information Processing Systems 24. Curran Associates, Inc., pp. 1341–1349.

Melo, E., Machado, D. M., Lisboa, R. C., Romeu, M. A. R., 2016. Overview of tide, wind and wave conditions along the Brazilian coast for coastal engineering practice. IX PIANCCOPEDEC, 9.

Milne, G. A., Mitrovica, J. X. 2008. Searching for eustasy in deglacial sea-level histories. Quaternary Science Reviews, 27(25-26), 2292-2302.

Milne, G.A., Long, A.J., Bassett, S.E., 2005. Modelling Holocene relative sea-level observations from the Caribbean and South America. Quat Sci Rev 24, 1183–1202. https://doi.org/10.1016/j.quascirev.2004.10.005

Peltier, W.R., Argus, D.F., Drummond, R., 2015. Space geodesy constrains ice age terminal deglaciation: The global ICE-6G_C (VM5a) model. Journal of Geophysical Research: Solid Earth 120, 450-487.

Pirazzoli, P. A. (1991). *World Atlas of Holocene Sea-Level Changes* (Vol. 58). Amsterdam, Elsevier (Elsevier Oceanography Series).

Porter, S.C., Stuiver, M., Heusser, C.J., 1984. Holocene Sea-Level Changes along the Strait of Magellan and Beagle Channel, Southernmost South America, Quaternary Research.

Prieto, A.R., Mourelle, D., Peltier, W.R., Drummond, R., Vilanova, I., Ricci, L., 2017. Relative sea-level changes during the Holocene in the Río de la Plata, Argentina and Uruguay: A review. Quaternary International 442, 35–49. https://doi.org/10.1016/j.quaint.2016.02.044

Rabassa, J., Coronato, A., Bujalesky, G., nica Salemme, M.H., Roig, C., Meglioli, A., Heusser, C., Gordillo, S., Roig, F., Borromei, A., Quattrocchio, M., 2000. Quaternary of Tierra del Fuego, Southernmost South America: an updated review.

Rasmussen, C., Williams, C., 2006. Gaussian Processes for Machine Learning. MIT Press, Cambridge, MA.

Reimer, P.J., Austin, W.E.N., Bard, E., Bayliss, A., Blackwell, P.G., Bronk Ramsey, C., Butzin, M., Cheng, H., Edwards, R.L., Friedrich, M., Grootes, P.M., Guilderson, T.P., Hajdas, I., Heaton, T.J., Hogg, A.G., Hughen, K.A., Kromer, B., Manning, S.W., Muscheler, R., Palmer, J.G., Pearson, C., Van Der Plicht, J., Reimer, R.W., Richards, D.A., Scott, E.M., Southon, J.R., Turney, C.S.M., Wacker, L., Adolphi, F., Büntgen, U., Capano, M., Fahrni, S.M., Fogtmann-Schulz, A., Friedrich, R., Köhler, P., Kudsk, S., Miyake, F., Olsen, J., Reinig, F., Sakamoto, M., Sookdeo, A., Talamo, S., 2020. The IntCal20 Northern Hemisphere Radiocarbon Age Calibration Curve (0-55 cal kBP). Radiocarbon 62, 725–757. https://doi.org/10.1017/RDC.2020.41

Reimer, P.J., Reimer, R.W., 2001. A marine reservoir correction database and On-line interface.

Ribeiro, S. R., Valadão, R. C., Gomes, M. O. S., Bittencourt, J. S., Alves, R. A., 2023. Paleoecological indicators of the highstand sea level on the Amazonian supralittoral until the last two millennia. Journal of South American Earth Sciences, 104422.

Ribolini, A., Aguirre, M., Baneschi, I., Consoloni, I., Fucks, E., Isola, I., Mazzarini, F., Pappalardo, M., Zanchetta, G., Bini, M., 2011. Holocene beach ridges and coastal evolution in the Cabo Raso bay (Atlantic Patagonian Coast, Argentina). J Coast Res 27, 973–983. https://doi.org/10.2112/JCOASTRES-D-10-00139.1

Rostami, K., Peltier, W.R., Mangini, A., 2000. Quaternary marine terraces, sea-level changes and uplift history of Patagonia, Argentina: comparisons with predictions of the ICE-4G

(VM2) model of the global process of glacial isostatic adjustment. Quat Sci Rev 19, 1496–1525.

Rovere, A., Antonioli, F., Bianchi, C. N. 2015. Fixed biological indicators. Handbook of Sea-Level Research, 268-280.

Rovere, A., Pappalardo, M., Richiano, S., Ryan, D. D., Rubio-Sandoval, K., Ruiz, P. M., Montes, A., Gowan, E. J. 2025. Reconstructing past sea-level changes from storm-built beach ridges. Geomorphology, 109659. https://doi.org/10.1016/j.geomorph.2025.109659

Rovere, A., Raymo, M.E., Vacchi, M., Lorscheid, T., Stocchi, P., Gómez-Pujol, L., Harris, D.L., Casella, E., O'Leary, M.J., Hearty, P.J., 2016. The analysis of Last Interglacial (MIS 5e) relative sea-level indicators: Reconstructing sea-level in a warmer world. Earth Sci Rev. https://doi.org/10.1016/j.earscirev.2016.06.006

Rovere, A., Ryan, D.D., Vacchi, M., Dutton, A., Simms, A.R., Murray-Wallace, C. V., 2023. The World Atlas of Last Interglacial Shorelines (version 1.0). Earth Syst Sci Data 15, 1–23. https://doi.org/10.5194/essd-15-1-2023

Rubio-Sandoval, K., Rovere, A., Cerrone, C., Stocchi, P., Lorscheid, T., Felis, T., Petersen, A.K., Ryan, D.D., 2021. A review of last interglacial sea-level proxies in the western Atlantic and southwestern Caribbean, from Brazil to Honduras. Earth Syst Sci Data 13, 4819–4845. https://doi.org/10.5194/essd-13-4819-2021

Rubio-Sandoval, K., Ryan, D. D., Richiano, S., Giachetti, L. M., Hollyday, A., Bright, J., Gowan, E., Pappalardo, M., Austermann, J., Kaufman, D., Rovere, A. 2024. Quaternary and Pliocene sea-level changes at Camarones, central Patagonia, Argentina. Quaternary Science Reviews 345. https://doi.org/10.1016/j.quascirev.2024.108999

Rutter, N., Radtke, U., Schnack, E. J., 1990. Comparison of ESR and amino acid data in correlating and dating Quaternary shorelines along the Patagonian coast, Argentina, Journal of Coastal Research, pp. 391–411.

Ryan, W. B. F., Carbotte, S. M., Coplan, J. O., O'Hara, S., Melkonian, A., Arko, R., Weissel, R. A., Ferrini, V., Goodwillie, A., Nitsche, F., Bonczkowski, J., Zemsky, R. 2009. Global Multi-Resolution Topography synthesis. Geochemistry, Geophysics, Geosystems, 10(3).

Santamaria-Aguilar, S., Schuerch, M., Vafeidis, A. T., Carretero, S. C., 2017. Long-term trends and variability of water levels and tides in Buenos Aires and Mar del Plata, Argentina. Frontiers in Marine Science, *4*, 380.

Schellmann, G., 2007. Bamberger geographische schriften herausgegeben von Heft 22 Teil I: Holozäne Meeresspiegelschwankungen-ESR-Datierungen aragonitischer Muschelschalen-Paläotsunamis. Institut für Gepgraphie an der Universitäat Bamberg, Bamberg.

Schellmann, G., Beerten, K., Radtke, U., 2008. Electron spin resonance (ESR) dating of Quaternary materials. E & G (Eiszeitalter u. Gegenwart). Quaternary Science Journal 57, 150–178.

Schellmann, G., Radtke, U., 2010. Timing and magnitude of Holocene sea-level changes along the middle and south Patagonian Atlantic coast derived from beach ridge systems, littoral

terraces and valley-mouth terraces. Earth Sci Rev 103, 1–30. https://doi.org/10.1016/j.earscirev.2010.06.003

Schellmann, G., Radtke, U., 2007. Zur ESR-Datierung holozäner sowie jung- bis mittelpleistozänerMuschelschalen—aktuelleMöglichkeitenundGrenzen. Bamberger Geographische Schriften 22, 113–152.

Schellmann, G., Radtke, U., 2003. Coastal Terraces and Holocene Sea-Level Changes along the Patagonian Atlantic Coast, Source: Journal of Coastal Research.

Schellmann, G., Radtke, U., 2000. ESR dating stratigraphically well-constrained marine terraces alongthe Patagonian Atlantic coast (Argentina).

Shennan, I., Long, A.J., Horton, B.P., 2015. Handbook of sea-level research: Framing research questions, in: Handbook of Sea-Level Research. Wiley Blackwell, pp. 3–25. https://doi.org/10.1002/9781118452547.ch2

Shennan, I., Bradley, S.L., Edwards, R., 2018. Relative sea-level changes and crustal movements in Britain and Ireland since the Last Glacial Maximum. Quat Sci Rev 188, 143–159. https://doi.org/10.1016/j.quascirev.2018.03.031

Shennan, I., Tooley, M.J., Davis, M.J., Andrew Haggart, B., 1993. Analysis and interpretation of Holocene sea-level data. Nature 302.

Smith, C., Salles, T., Concejo, A. V., 2020. pyReefmodel/RADWave: RADWave: Python code for ocean surface wave analysis by satellite radar altimeter.

Souza, M.C., Angulo, R.J., Pessenda, L.C.R., 2001. Evolução geológica e paleogeográfica da planície costeira de Itapoá, litoral norte de Santa Catarina. Revista Brasileira de Geociências 31, 223–230.

Spada, G., Stocchi, P., 2007. SELEN: A Fortran 90 program for solving the "sea-level equation". Computers & Geosciences 33, 538–562.

Spotorno, P., Tâmega, F. T., Bemvenuti, C. E. 2012. An overview of the recent vermetids (Gastropoda: Vermetidae) from Brazil. Strombus, 19(1/2), 1.

Stuiver, M., Polach, H.A., 1977. Discussion Reporting of 14 C Data. Radiocarbon 19, 355–363. https://doi.org/10.1017/s0033822200003672

Suguio, K., Flexor, J.M., Nacional, O., 1980. Le Quaternaire marin brésilien (Littoral pauliste, sud fluminense et bahianais).

Suguio, K., Martin, L., 1978. Formaçoes quaternarias marinhas do litoral paulista e sul fluminense = quaternary marine formations of the state of Sao Paulo and Southern Rio de Janeiro.

Suguío, K., Martin, L., Bittencourt, A. C., Dominguez, J. M., Flexor, J. M., de Azevedo, A. E. 1985. Flutuações do nível relativo do mar durante o Quaternário Superior ao longo do litoral brasileiro e suas implicações na sedimentação costeira. *Revista Brasileira de Geociências*, *15*(4), 273-86.

Sulzbach, R., Klemann, V., Knorr, G., Dobslaw, H., Dümpelmann, H., Lohmann, G., Thomas, M., 2023. Evolution of Global Ocean Tide Levels Since the Last Glacial Maximum. Paleoceanogr Paleoclimatol 38. https://doi.org/10.1029/2022PA004556

Styron, R. 2019. GEMScienceTools/gem-global-active-faults: First release of 2019.

Tamura, T., 2012. Beach ridges and prograded beach deposits as palaeoenvironment records. Earth Sci Rev. https://doi.org/10.1016/j.earscirev.2012.06.004

Tan, F., Khan, N. S., Li, T., Meltzner, A. J., Majewski, J., Chan, N., Chutcharavan, P., Cahill, N., Vacchi, M., Peng, D., Horton, B. P. 2023. Holocene relative sea-level histories of far-field islands in the mid-Pacific. Quaternary Science Reviews, 107995.

Thompson, S. B., Creveling, J. R., 2021. A global database of marine isotope substage 5a and 5c marine terraces and paleoshoreline indicators. Earth System Science Data, 13(7), 3467-3490.

Toniolo, T., Giannini, P. C. F., Angulo, R. J., de Souza, M. C., Pessenda, L. C. R., Spotorno-Oliveira, P., 2020. Sea-level fall and coastal water cooling during the Late Holocene in Southeastern Brazil based on vermetid bioconstructions. Marine Geology, 428, 106281.

Törnqvist, T.E., Rosenheim, B.E., Hu, P., Fernandez, A.B., 2015. Radiocarbon dating and calibration, in: Handbook of Sea-Level Research. Wiley Blackwell, pp. 347–360. https://doi.org/10.1002/9781118452547.ch23

Tushingham, A.M., Peltier W.R., 1992. Validation of the ICE-3G Model of Würm-Wisconsin Deglaciation Using a Global Data Base of Relative Sea Level Histories. Journal of Geophysical Research: Atmospheres, 97(B3), 3285-3304. doi: 10.1029/91JB02176

US Geological Survey, E. H. P. (2017). Advanced National Seismic System (ANSS) comprehensive catalog of earthquake events and products: Various.

Vacchi, M., Engelhart, S.E., Nikitina, D., Ashe, E.L., Peltier, W.R., Roy, K., Kopp, R.E., Horton, B.P., 2018a. Postglacial relative sea-level histories along the eastern Canadian coastline. Quat. Sci. Rev. 201, 124e146. https://doi.org/10.1016/j.quascirev.2018.09.043.

van Andel, T.H., Laborel, J., 1964. Recent high relative sea level stand near Recife, Brazil. Science (1979) 145, 580–581. https://doi.org/10.1126/science.145.3632.580

van de Plassche, O., 1986. Sea-level research: a manual for the collection and evaluation of data. Geo Books, Norwich.

Vos, K., Harley, M. D., Splinter, K. D., Walker, A., Turner, I. L., 2020. Beach slopes from satellite-derived shorelines. Geophysical Research Letters 47(14), e2020GL088365. e2020GL088365 2020GL088365.

Vos, K., Splinter, K. D., Harley, M. D., Simmons, J. A., Turner, I. L., 2019. Coastsat: A google earth engine-enabled python toolkit to extract shorelines from publicly available satellite imagery. Environmental Modelling Software 122, 104528.

Zanchetta, G., Bini, M., Isola, I., Pappalardo, M., Ribolini, A., Consoloni, I., Boretto, G., Fucks, E., Ragaini, L., Terrasi, F., 2014. Middle- to late-Holocene relative sea-level changes at

Puerto Deseado (Patagonia, Argentina). Holocene 24, 307–317. https://doi.org/10.1177/0959683613518589

Zanchetta, G., Consoloni, I., Isola, I., Pappalardo, M., Ribolini, A., Aguirre, M., Fucks, E., Baneschi, I., Bini, M., Ragaini, L., Terrasi, F., Boretto, G., 2012. New insights on the Holocene marine transgression in the Bahía Camarones (Chubut, Argentina). Italian Journal of Geosciences 131, 19–31. https://doi.org/10.3301/IJG.2011.20

Supplementary material

Spatio-Temporal Empirical Hierarchical Model

The STEHM has three levels: 1) a data level, which models the way different SLIPs record RSL with vertical and temporal noise; 2) a process level, which distinguishes between RSL changes that are common across the full database and those that are confined to the specific regions; and 3) a hyperparameter level, which characterizes prior expectations regarding dominant spatial and temporal scales of RSL variability (Khan et al., 2022). At the data level, we observe noisy RSL y_i and noisy age t_i:

$$y_i = f(x_i, t_i) + \epsilon^y_i + w(x_i, t_i) + y_0(x_i) \quad (1)$$

$$t_i = \hat{t}_i + \epsilon^t_i \quad (2)$$

where x_i and t_i are the geographic location and true age, respectively, of observations indexed by i; $f(x_i, t_i)$ is the true RSL value at x_i and t_i; ϵ_i^y is the vertical error of each RSL data point (assumed to be independent and normally distributed); $w(x_i, t_i)$ is a supplemental white noise term that accounts for variations in the data that cannot be explained by the terms in the process-level model; $y_0(x_i)$ is a site-specific datum offset to ensure that RSL data can be directly compared. $\hat{t}_i$ is the mean estimated age of each RSL data point, and ϵ_i^t is its error. The age uncertainties are incorporated using the noisy-input Gaussian Process (GP) method of McHutchon and Rasmussen (2011), which uses a first-order Taylor-series approximation to translate errors in the independent variable into equivalent errors in the dependent variable:

$$f(x_i, t_i) \approx f(x_i, \hat{t}_i) + \epsilon^t_i \frac{\partial f(\hat{x_i}, \hat{t_i})}{\partial t} \quad (3)$$

At the process level, we model the sea-level field, $f(x_i, t_i)$, as the sum of two component fields, $f(x, t) = r(t) + l(x, t)$, where x represents geographic location and t represents time. The two components are: a common regional term, $r(t)$, representing the time-varying signal shared by all sites included in the analysis, and a local term, $l(x, t)$, representing site-specific processes. The priors for each term in the model are mean-zero Gaussian processes (Rasmussen and Williams, 2006) with 3/2 Matérn covariance functions (see Ashe et al., 2019 for more details). Hyperparameters defining prior expectations of the amplitudes and spatio-temporal scales of variability were estimated through maximum-likelihood optimization (Supplementary Table 1).

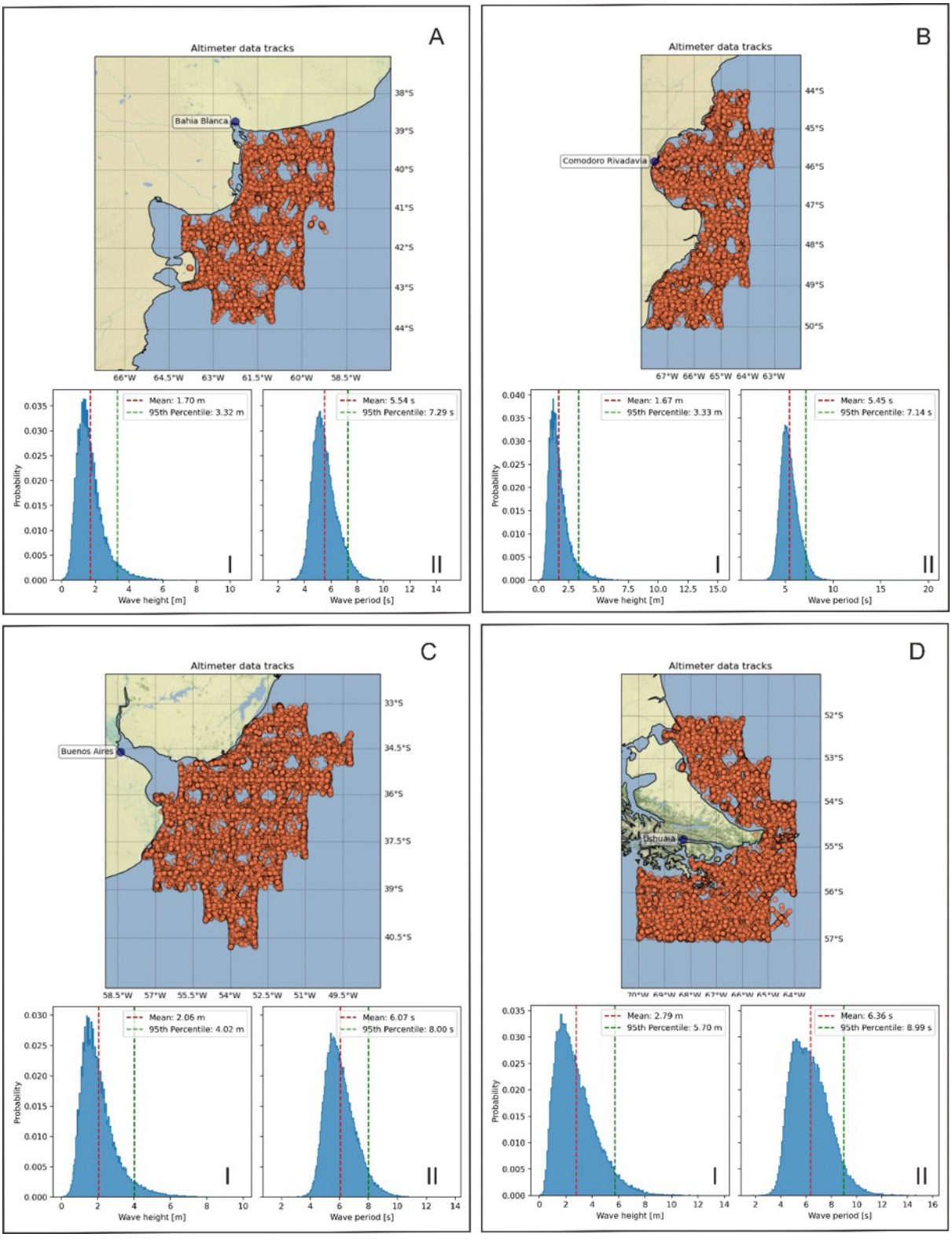

Supplementary Figure 1. Maps of satellite altimetry tracks extracted from offshore wave conditions (IMOS, 2023). A) Bahia Blanca, B) Comodoro Rivadavia, C) Buenos Aires, D) Ushuaia; I) and II) respectively, histograms of wave height and period per region.

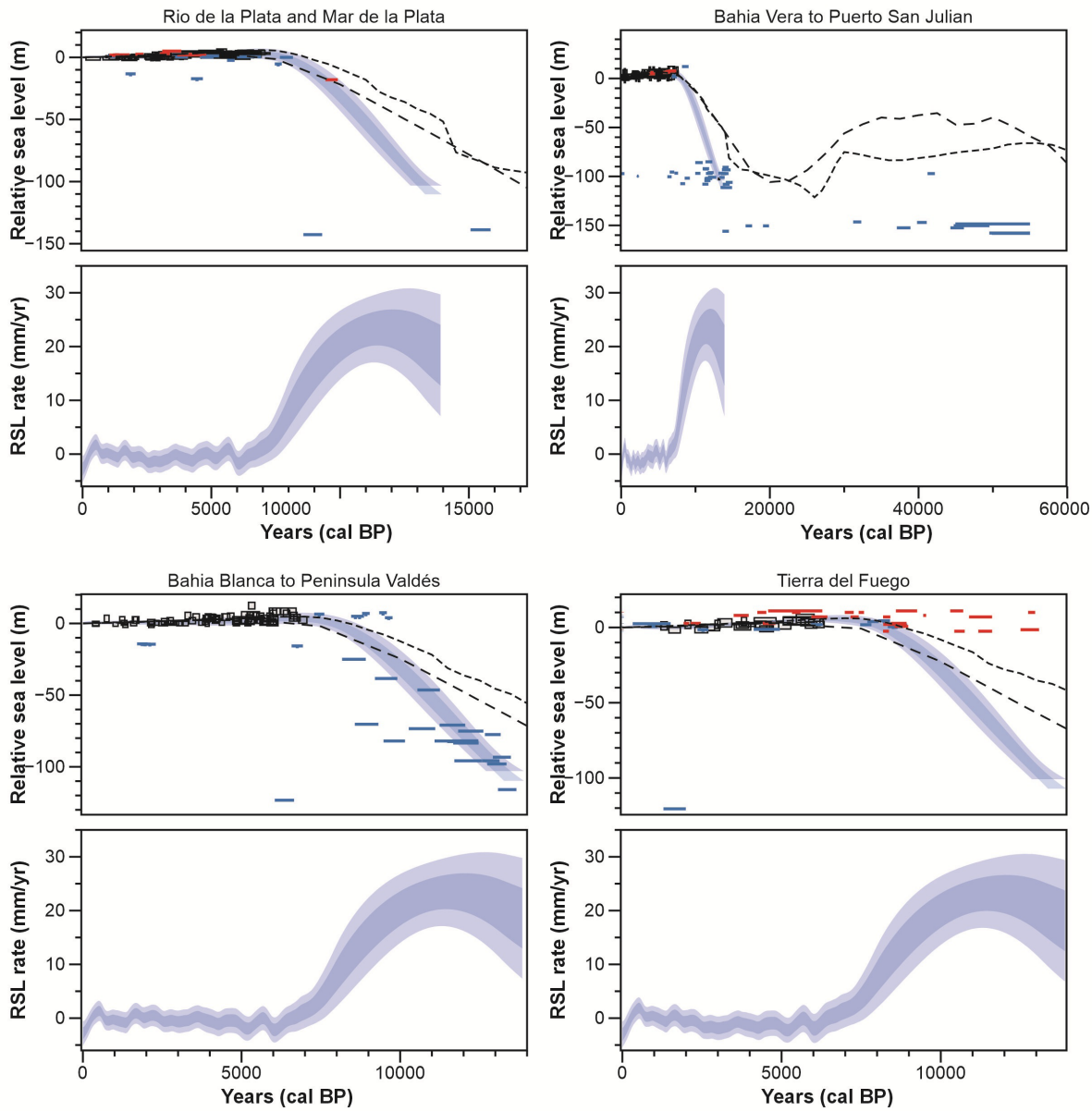

Supplementary Figure 2. RSL reconstructions and rates from regions 9, 10, 11, and 12 using the spatio-temporal model. For all plots, the model mean and 2σ uncertainty are represented by a solid line and shaded envelopes, respectively. Index points (grey boxes) are plotted as calibrated age against changes in sea level relative to the present. Limiting points are plotted as an "inverted-T" red symbol for terrestrial or an "T" blue symbol for marine. The dimensions of boxes and symbols for each point are based on elevation and age (2σ) errors. SLIP: sea-level index point; STEHM: spatio-temporal empirical hierarchical model; ICE6G (large, dashed line) and PaleoMIST (short, dashed line) represent the GIA models.

Supplementary Table 1. Hyperparameters for the spatio-temporal empirical hierarchical model.

Hyperparameters	**Tuned value**
Global amplitude (mm)	114822.864
Global temporal parameter (years)	24387.0275
Linear amplitude	0.27247905
Linear geographic length scale (angular degrees)	0.04563275
Regional amplitude (mm)	1387.38685
Regional temporal parameter (years)	1663.64684
Regional geographic length scale (angular degrees)	3.33973316
Local amplitude (mm)	1.40687193
Local temporal parameters (year)	1.44688715
Local geographic length scale (angular degrees)	0.88282792
White noise (mm)	0.14805049